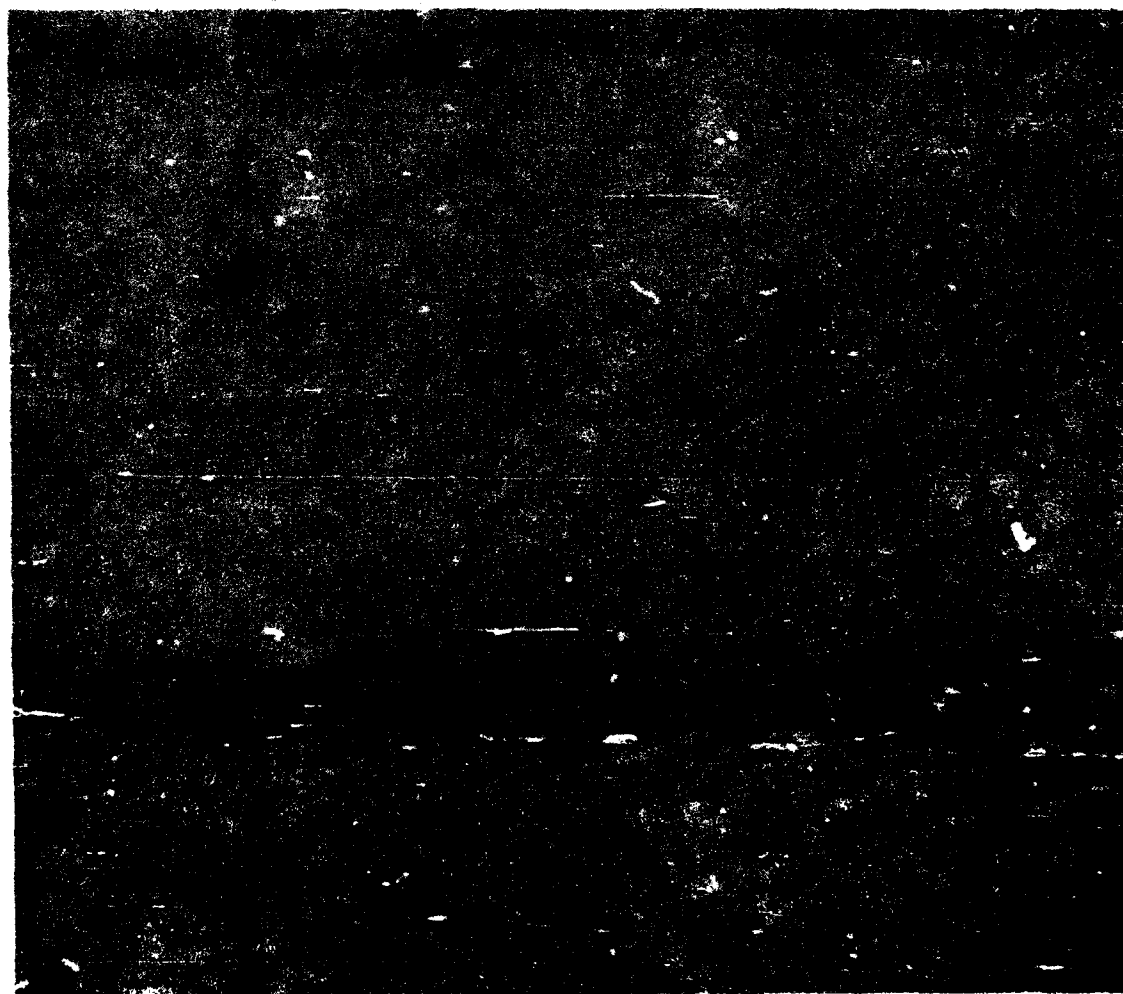# CSL COORDINATED SCIENCE LABORATORY

STRUCTURE AND ELECTRICAL PROPERTIES OF RF SPUTTER DEPOSITED INDIUM ANTIMONIDE THIN FILMS

UNIVERSITY OF ILLINOIS – URBANA, ILLINOIS

REPORT DOCUMENTATION PAGE		READ INSTRUCTIONS BEFORE COMPLETING FORM
1. REPORT NUMBER	2. GOVT ACCESSION NO.	3. RECIPIENT'S CATALOG NUMBER
4. TITLE (and Subtitle) STRUCTURE AND ELECTRICAL PROPERTIES OF RF SPUTTER DEPOSITED INDIUM ANTIMONIDE THIN FILMS,		5. TYPE OF REPORT & PERIOD COVERED Technical Report
		6. PERFORMING ORG. REPORT NUMBER R-705; UILU-ENG-2241
7. AUTHOR(s) Charles Edward Wickersham, Jr.		8. CONTRACT OR GRANT NUMBER(s) DAAB-07-72-C-0259
9. PERFORMING ORGANIZATION NAME AND ADDRESS Coordinated Science Laboratory University of Illinois at Urbana-Champaign Urbana, Illinois 61801		10. PROGRAM ELEMENT, PROJECT, TASK AREA & WORK UNIT NUMBERS
11. CONTROLLING OFFICE NAME AND ADDRESS Joint Services Electronics Program		12. REPORT DATE Dec 1975
		13. NUMBER OF PAGES 62
14. MONITORING AGENCY NAME & ADDRESS(if different from Controlling Office)		15. SECURITY CLASS. (of this report) UNCLASSIFIED
		15a. DECLASSIFICATION/DOWNGRADING SCHEDULE

16. DISTRIBUTION STATEMENT (of this Report)

Approved for public release; distribution unlimited

17. DISTRIBUTION STATEMENT (of the abstract entered in Block 20, if different from Report)

18. SUPPLEMENTARY NOTES

19. KEY WORDS (Continue on reverse side if necessary and identify by block number)

Indium Antimonide
RF Sputtering
Thin Films

20. ABSTRACT (Continue on reverse side if necessary and identify by block number)

During the last few years, sputtering has become a very important industrial technique for depositing thin films. Typical applications include metalization and passivation in the electronics industry, the deposition of complex cermets, glasses, and plastics, and the formation of coatings for corrosion, abrasion, and wear resistance. However, relatively little work has been reported on the growth of compound semiconducting films by sputtering.

DD FORM 1 JAN 73 1473   EDITION OF 1 NOV 65 IS OBSOLETE

STRUCTURE AND ELECTRICAL PROPERTIES OF RF SPUTTER
DEPOSITED INDIUM ANTIMONIDE THIN FILMS

by

Charles Edward Wickersham, Jr.

STRUCTURE AND ELECTRICAL PROPERTIES OF RF
SPUTTER DEPOSITED INDIUM ANTIMONIDE THIN FILMS

BY

CHARLES EDWARD WICKERSHAM JR.
B.S., Rose-Hulman Institute of Technology, 1973

THESIS

Submitted in partial fulfillment of the requirements
for the degree of Master of Science in Metallurgical Engineering
in the Graduate College of the
University of Illinois at Urbana-Champaign, 1976

Thesis Advisor: Professor Joseph E. Greene

Urbana, Illinois

ACKNOWLEDGMENT

TABLE OF CONTENTS

LIST OF TABLES

I. INTRODUCTION

During the last few years, sputtering has become a very important industrial technique for depositing thin films. Typical applications include metalization and passivation in the electronics industry, the deposition of complex cermets, glasses, and plastics, and the formation of coatings for corrosion, abrasion, and wear resistance. However, relatively little work has been reported on the growth of compound semi-conducting films by sputtering.

Sputtering as a growth technique for compound, ternary, and quaternary semiconductors has several advantages over other growth techniques. It is a physical as opposed to a chemical process and as such does not depend on the melting point or vapor pressure of elemental constituents in the target. Control over film chemical composition and growth rate can be obtained by adjusting deposition parameters such as applied power, sputtering gas composition and pressure, substrate temperature, and substrate bias.

A III-V compound semiconductor was chosen for this investigation for several reasons. The large difference between the melting points and vapor pressures of the group three and group five components makes this class of materials attractive for evaluating film stoichimetry over a broad range of sputtering conditions. In addition, III-V compound films are important electronic device materials. The room temperature band gaps of the III-V compounds vary from 3.39 eV for GaN to 0.17 eV for InSb. The bulk electron mobilities vary from 200 cm^2/V-sec in AlSb to 72,000 cm^2/V-sec in InSb. InSb was chosen for this investigation since its low melting point

(525°C) should allow low structural transition temperatures
(amorphous→polycrystalline→epitaxial→single crystal) during growth. Also
the small band gap and high electron mobility of InSb makes the electrical
properties of this material particularly sensitive to changes in micro-
structure and stoichiometry.

This thesis presents the results of an investigation of the
properties of RF sputter deposited InSb. The metallurgical and electronic
properties of deposited films were determined as functions of growth
parameters such as deposition rate, target bias, argon pressure, substrate
temperature, and substrate bias. A large number of InSb samples were
grown on BaF_2, CaF_2, NaCl, and NaI single crystal substrates in addition
to glass microscope slides. The microstructure and orientation of the
films were observed using transmission electron microscopy. The chemical
stoichiometry of the films was determined by Auger electron spectroscopy.
Film resistivity and Hall mobility were measured on polished and annealed
(p-a) CaF_2 substrates. The electrical properties of these films were
related to their structure and growth conditions so that the dominant charge
scattering mechanism could be identified.

A summary of the literature on the deposition and properties of
thin film InSb is presented in Chapter II. Chapter III describes the
experimental procedures and equipment used in this investigation, while
Chapter IV contains the experimental results which are separated into five
sections. The first of these deals with deposition rate and thickness
control of RF sputtered InSb. The second and third sections present the

results of crystallographic and chemical examination of the films as a
function of growth conditions and substrate material. The fourth section
in Chapter IV presents the results of the electrical measurements, while
the final section describes the effects of applying an RF bias to the
substrate during the deposition of the film. Chapter V is a discussion
of the experimental results, and Chapter VI contains the conclusions
and suggestions for further work.

II. BACKGROUND

Techniques which have been reported for the deposition of InSb films include flash evaporation,[1] three source thermal evaporation,[2] liquid phase epitaxy,[3] and DC sputtering.[4] An excellent review of the literature up to and including 1967 is given by Wieder.[5] The present review will summarize only those investigations in which sputtering was used to deposit III-V compounds or in which relevant information on the structure or physical properties of III-V compound thin films was presented.

Richards, Hart, and Mueller[1] investigated the flash evaporation of several III-V compounds onto single crystal germanium and cleaved CaF_2 substrates. They observed orientated growth of InSb on germanium at a substrate temperature of $200^{\circ}C$, epitaxy with twinning in the range $250^{\circ}C$ to $300^{\circ}C$, and untwinned epitaxy between $300^{\circ}C$ and $400^{\circ}C$. Similar results were obtained with cleaved CaF_2 substrates, but structural transition temperatures were not reported. Deposition rates in these experiments ranged between 600 and 6000 $\overset{\circ}{A}$/min.

The first published results on the deposition of III-V compound films by DC sputtering were reported by Moulton[4] who deposited InSb and GaSb onto fused silica. He found a maximum InSb electron mobility of 460 cm^2/V-sec for a 4000 $\overset{\circ}{A}$ film grown at $250^{\circ}C$. Cervenak[6,7] has made an extensive investigation of the structure and electrical properties of DC sputtered InSb films. He identified the mobility limiting mechanism in cathodic sputtered InSb thin films as dislocation barrier scattering[7] and

observed that the films were polycrystalline with texture when deposited on NaCl in the temperature range 270°C to 350°C. He also reported that the transition from textured to monocrystalline films occurred between 350°C and 420°C for deposition rates of ~ 40 Å/min.

Kahn[8] performed in situ reflection electron diffraction studies of DC sputtered InSb on NaCl. He reported amorphous films at substrate temperatures of 25°C with complete epitaxy occurring above 250°C. A thin epitaxial layer of tetragonal indium formed at the substrate-film interface and InSb was not detected until the film reached a thickness of 32 Å. Kahn suggested that the indium forms in the initial stages of growth due to the high vapor pressure of the antimony. The epitaxial relationship between the InSb and NaCl was $(100)_{NaCl} \parallel (100)_{InSb}$.

Eckenbach, Fuhs, and Stuke[9] have studied the growth and electrical properties of amorphous InSb deposited by flash evaporation onto glass, quartz, CaF_2, and KBr substrates. They found that the room temperature band gap of amorphous InSb is shifted upwards from 0.17 eV in crystalline InSb to 0.65 eV in amorphous InSb.

Ling, Fisher, and Anderson[10] deposited InSb on mica substrates by flash evaporation. At a substrate temperature of 380°C they obtained films with an average grain size of only 100 Å. After annealing at 400°C for 3 hours, the grains were on the order of the film thickness, 3000 Å. The electron mobilities of the annealed films were $\sim 2 \times 10^3$ cm^2/V-sec and the temperature dependence of the mobility was similar to that reported by Cervenak.

Clawson[11] has produced n-type InSb films with bulk-like electron mobilities (72,000 cm^2/V-sec) and net carrier concentrations of 7×10^{15} cm^{-3} by hot wire zone recrystallization. The films were deposited by evaporation onto glass substrates and then heated in air for 30 minutes at 300°C to form a protective indium oxide layer over the film. The film was then recrystallized by zone melting in 99.99% pure helium gas.

Several authors[12,13] have shown that the deposition rate plays an important role in determining the crystallinity of DC sputtered germanium films. Khan[13] found that adsorbed oxygen on germanium substrates also plays an important role in determining the epitaxial temperature. Burton and Day[14] sputter deposited ZnS and GaAs onto cleaved NaCl single crystals. They reported a significant reduction in the epitaxial temperature of GaAs on NaCl when using RF sputtering as compared with vacuum evaporation and DC sputtering.

III. EXPERIMENTAL PROCEDURE

This chapter contains a detailed description of the substrate and sample preparation procedures, in addition to techniques used to measure the deposition rate and physical properties of the deposited films. The experimental apparatus used in these experiments is also described.

III.A. Substrate Preparation

The substrates used in these experiments were: cleaved CaF_2, BaF_2, NaCl, and NaI wafers; polished and annealed CaF_2 wafers; and glass microscope slides. The salts were obtained from the Harshaw Chemical Company in the form of single crystal boules with the cleavage face perpendicular to the long axis. Cleavage was carried out in air immediately prior to insertion into the vacuum system. During runs in which several types of substrates were used, the substrates were cleaved in order of increasing hygroscopic tendency (i.e. CaF_2, BaF_2, NaCl, and NaI). The surface area of the cleaved wafers was approximately 1 cm^2.

All electrical measurements on InSb films were made on samples deposited on polished and annealed p-a CaF_2 substrates. CaF_2 was chosen since it is the least hygroscopic and can be easily polished. It was found that the electron mobilities of thin InSb films grown on cleaved substrates were limited by scattering from replicated cleavage steps whose height was on the order of the film thickness. The p-a CaF_2 substrates were prepared by slicing 0.2 cm thick (111) oriented wafers from the boule using a diamond saw. The estimated misorientation of the wafers after cutting

and polishing was $\pm 2^{\circ}$. Final polishing was carried out on beeswax using 0.03 micron alumina grit suspended in methanol. The wafers were then rinsed in trichloroethylene, acetone, and methanol; dried with tank nitrogen; and annealed in a vacuum of 10^{-6} Torr for 30 minutes at $900^{\circ}C$ to remove surface damage.[15] The p-a CaF_2 substrates were then stored in a desiccator until needed.

A list of the orientations and lattice constants of the substrates used in these experiments is given in Table 1. The film-substrate mismatch has been calculated from the following equation

$$M = 100 \times (a_{o\ InSb} - a_{o\ sub})/a_{o\ sub} \qquad (3.1)$$

and is also given in Table 1. In equation (3.1) M is the percent lattice mismatch and $a_{o\ InSb}$ and $a_{o\ sub}$ are the lattice constants for InSb and the substrate respectively.

Films were also deposited on glass microscope slides during each run to determine deposition rates and film thickness. The method used for cleaning the glass slides is given in the Appendix.

III.B. InSb Film Deposition

The InSb films were grown in a modified Perkin-Elmer Ultek 2400-J RF sputtering system. The substrates were supported on a rotatable table which contains a carbon filament heater capable of $700^{\circ}C$. The substrates could also be RF sputter etched prior to deposition and RF bias sputtered during deposition. The 10.16 cm diameter water-cooled InSb target was purchased from the Haselden Company and was mounted on a 10 centimeter diameter OFHC copper backing plate with a silver based epoxy supplied by

TABLE 1

List of Substrates Used in These Experiments

Substrate	Surface	Lattice Constant (Å)	% Mismatch InSb-Substrate
CaF$_2$	c(111)*	5.46	18.5
CaF$_2$	p-a(111)**	5.46	18.5
BaF$_2$	c(111)	6.20	4.35
NaCl	c(100)	5.64	14.7
NaI	c(100)	6.475	0.5

---

*c(111) denotes a (111) type cleavage face.

**p-a(111) denotes a polished and annealed (111) surface.

Cerac Inc. A 4.1 cm target to substrate separation was maintained during all experiments and the target bias voltage (peak to peak at 13.56 MHz), forward power, and reverse power were monitored. The substrate assembly was grounded, but films grown on insulating substrates were electrically floating.

The heater temperature was calibrated using a chromel-alumel thermocouple in good thermal contact with the substrate table. The substrate temperature increase during sputtering was measured with a chromel-alumel thermocouple attached to the upper surface of a polished CaF_2 substrate using a silver based thermally conductive epoxy marketed by Cerac Inc. Figure 1 shows the temperature of the substrate as a function of time and applied target bias with the heater off. The increase in temperature is due primarily to bombardment by energetic secondary electrons emitted by the target and to plasma radiation. The stainless steel heater plate was precoated with approximately one micron of InSb to reduce contamination of the deposited film by secondary sputtering during deposition. All contact masks were also coated with InSb.

A typical operational cycle included mechanical rough pumping of the chamber to 2×10^{-2} Torr followed by turbomolecular pumping (Leybold Heraeus Turbovac 350) to the mid 10^{-7} Torr range. This base pressure was typically obtained in under four hours with a LN_2 cold trap between the bell jar and the pumps. High purity argon was passed through a scrubber, which consisted of titanium sponge heated to $900^{\circ}C$, before being leaked into the sputtering chamber. The system was purged for
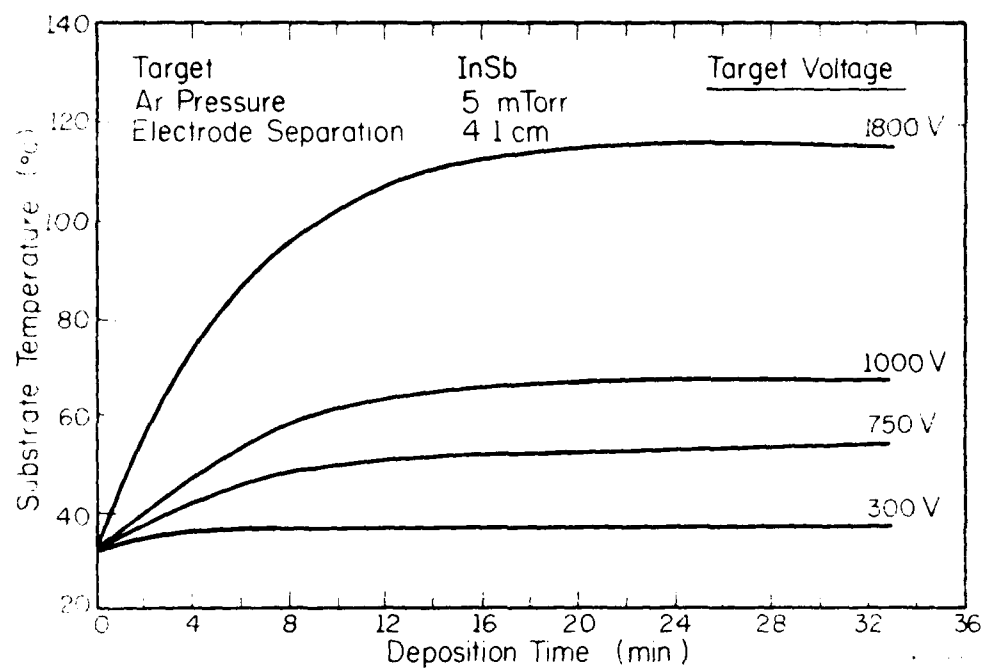
Figure 1. The substrate temperature as a function of
sputter deposition time for an Ar pressure
of 5 mTorr.

approximately fifteen minutes prior to igniting the plasma. It was found

that the plasma could not be formed at argon pressures below 8×10^{-3} Torr,

but once a discharge existed the pressure could be reduced to less than

5×10^{-3} Torr while maintaining a stable discharge. The target was

always sputter cleaned with the substrates in a blank position for a

minimum of five minutes prior to rotating the substrate table under the

target and beginning deposition. After a predetermined length of time the

target bias was removed and the argon inlet valve was closed. Tank nitrogen

was used to vent the bell jar after the samples were allowed to cool

overnight.

Deposition rates were determined by interferometrically measuring

the thickness of films deposited on glass slides for a known length of time.

The thickness of the samples used for the electrical measurements was

also checked by both gravimetric and surface profiling techniques. All

thickness measurements agreed to within 10%.

III.C. Metallurgical Measurements

The microstructure and texture of RF sputtered InSb films were

determined using a 200 KV JEOL transmission electron microscope. Films

grown on NaCl and NaI were prepared for examination by dissolving the

substrates in deionized water and then catching the floating film on copper

grids. Films grown on BaF_2 and CaF_2 were separated from the substrates

by first dipping the samples in a heated solution of 35% HCl and then

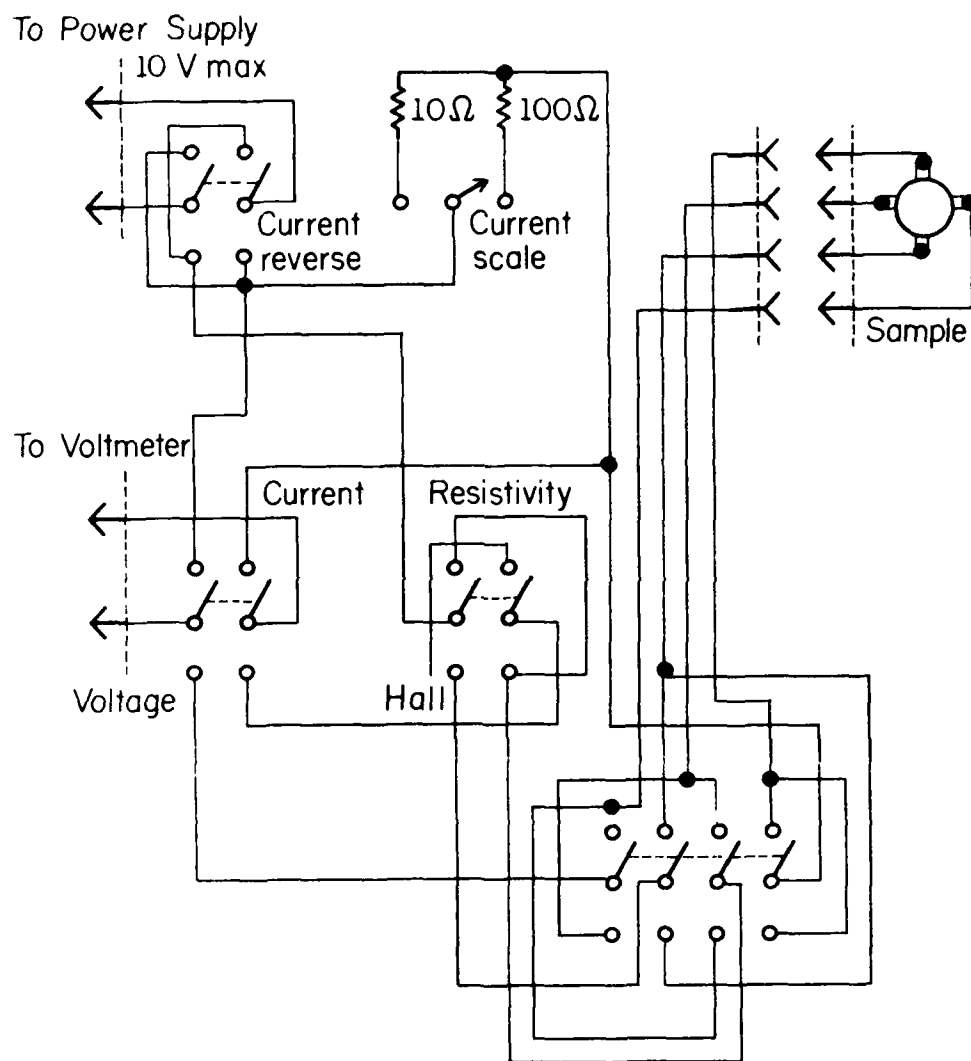floating the film off in deionized water.

The grain size of the film was determined by a method suggested by Williamson.[16] A series of random lines are drawn on the micrograph and the average crystallite size is then determined from the relation

$$d = \Sigma L / \Sigma N \qquad (3.2)$$

where ΣL is the total length of the lines used and ΣN is the total number of grain boundaries the line intersects. The total line distance used for determining the average grain size was 50 cm on a 7 cm x 12.5 cm micrograph with a magnification of 35,000 x.

III.D. Electrical Measurements

The resistivity and Hall coefficients of deposited films were determined by the van der Pauw technique.[17] Figure 2 shows a schematic diagram of the switching circuit which was designed for these measurements. A reversible magnetic field of 3.9 kilogauss was used. Low temperature measurements were made with a heated cold finger in a liquid nitrogen dewar. The CaF_2 substrates were fastened to the cold finger with a thermally conductive micropaint marketed by Micro-circuits Company, New Buffalo, Michigan. The sample temperature was measured with a copper-constantan thermocouple connected to the CaF_2 substrate with the silver micropaint. The van der Pauw pattern was produced either by contact masking during deposition or by photolithographic techniques after deposition. A 1:1 solution of 0.1 N potassium ferrocyanide and 35% HCl acid was used as the etchant in the photolithographic technique. Ohmic contacts to the films were formed using the silver micropaint.

To Power Supply
10 V max

10 Ω   100 Ω

Current
reverse

Current
scale

Sample

To Voltmeter

Current

Resistivity

Voltage

Hall

KP – 963

Figure 2. A schematic diagram of the circuit used in making
van der Pauw resistivity and Hall coefficient
measurements.

III.E. Chemical Analysis

A Physical Electronics Auger electron spectrometer was used for the chemical analysis of the films. The samples were placed in the system which was then evacuated to 10^{-9} Torr. Sample surface contamination was removed prior to analysis by a short ion beam etch at an argon pressure of 5×10^{-5} Torr. The stoichiometry of InSb films grown under different conditions was estimated by comparing the ratio of the differen- tiated peak to peak auger intensities of the indium and antimony peaks in the films with the peak ratio in a stoichiometric bulk InSb specimen.

III.F. RF Substrate Biasing

The effects on the metallurgical and electronic properties of deposited films of both sputter etching the substrates prior to deposition and film deposition in the RF bias mode were evaluated. Selected substrates were sputter etched at either -250 V or -500 V for ten minutes after which they were annealed at $400^{\circ}C$ for 60 minutes prior to deposition to reduce ion damage effects. Substrate bias deposition was accomplished by splitting the input RF power between the target and the substrates.

IV. EXPERIMENTAL RESULTS

The effects of substrate temperature, argon pressure, and RF substrate bias on InSb deposition rate are summarized in the first section of this chapter. The next two sections contain the results of microstructural and chemical analysis of deposited films. Electrical measurements are presented in section IV.D. Finally the effects of substrate sputter cleaning prior to deposition and RF-bias sputtering are described.

IV.A. Deposition Rate

The deposition rate of InSb as a function of target bias voltage for various substrate temperatures and argon pressures is given in Figure 3. The target bias voltage can be related to the deposition rate by the empirical relation

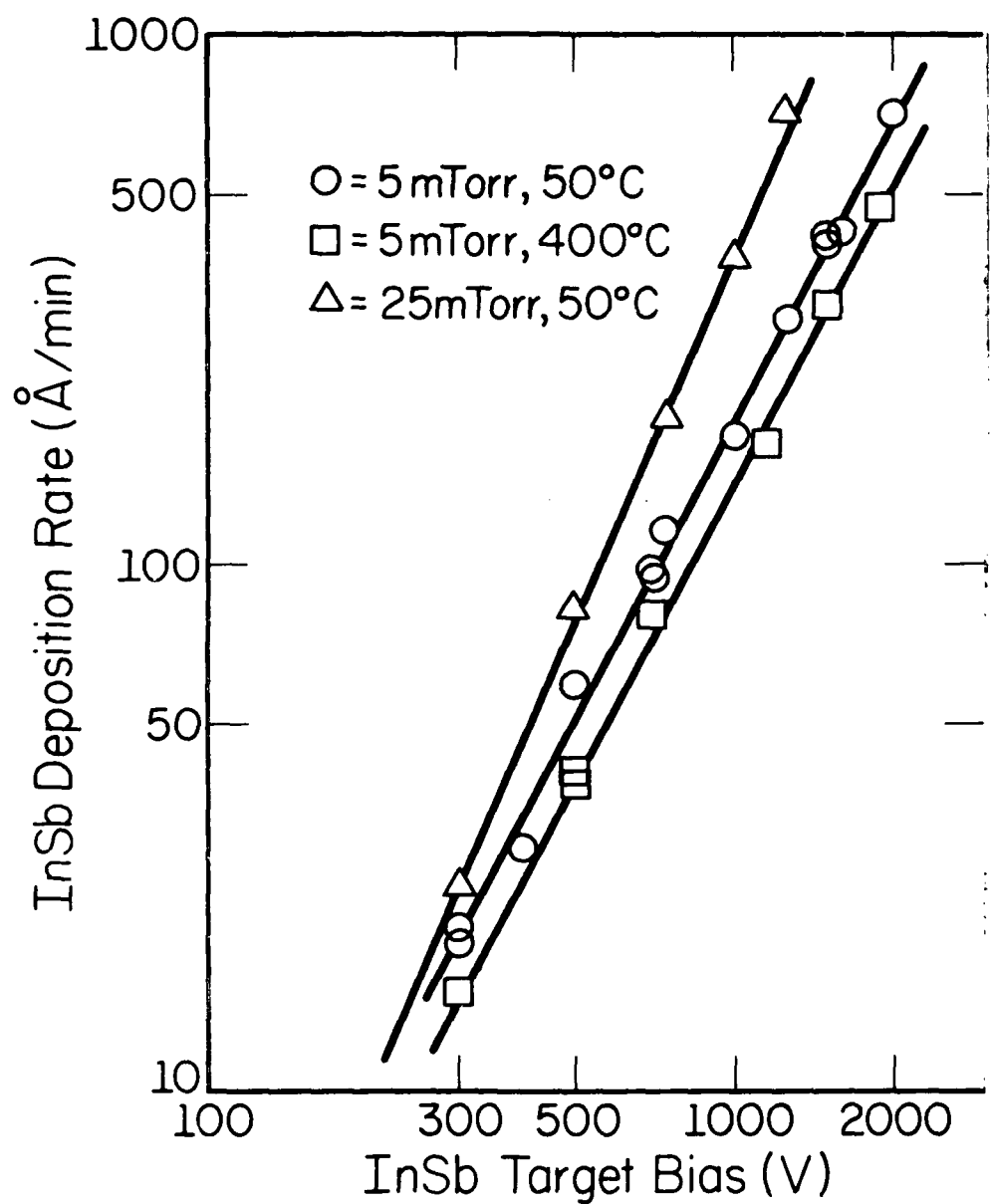$$R = R_o (V - V_c)^b \qquad (4.1)$$

where V is the target bias voltage, V_c is the sputtering threshold for InSb (approximately 25 V), b is a function of argon pressure only, and R_o is the rate coefficient which depends on both the substrate temperature and argon pressure. Table 2 lists the observed values of b and R_o as a function of substrate temperature and argon pressure for RF sputtered InSb deposited with a target to substrate separation of 4.1 cm.

It can be seen from Figure 3 and Table 2 that the rate coefficient is slightly dependent on the substrate temperature. Throughout this thesis substrate temperature will refer to the initial temperature of the substrate.

TABLE 2

Values of Deposition Coefficients for InSb

Ar Pressure (mTorr)	Substrate Temperature (°C)	b	R
5	50	1.80	7.8×10^{-4}
10	50	1.98	3.1
15	50	2.14	1.3
20	50	2.22	.83
25	50	2.34	.37
5	300	1.84	5.1
5	400	1.84	4.6

Figure 3.   InSb deposition rate as a function of target bias
voltage for sputtering pressures of 25 mTorr and
5 mTorr and substrate temperatures of 50°C and 400°C.

The reduction in deposition rate with increased substrate temperature is due to a reduction in the sticking coefficients of the incoming indium and antimony atoms. Further discussion of this effect is given in Chapter V.

Figure 4 shows more clearly that increasing the sputtering pressure at constant target bias voltage and substrate temperature results in an increase in the film deposition rate. As the pressure is increased, a critical saturation pressure is reached after which the deposition rate is independent of pressure. This critical saturation pressure increases slightly as the target bias is increased.

The application of an RF substrate bias during deposition also affects the InSb deposition rate as shown in Figure 5. Because of impedance matching and power splitting difficulties, experimental data could not be obtained for substrate to target bias ratios less than 0.075. Hence the curves are dotted in this region and are drawn to follow the general theoretical predictions of Cuomo et. al.[18] The results show that R increases initially at low RF bias, reaches a maximum, and decreases at higher bias voltages. It is possible to choose a bias voltage such that for a given target voltage the deposition rate remains the same as that obtained with no substrate bias.

IV.B. Film Structure

Using transmission electron microscopy, six distinct microstructures were observed in RF sputtered InSb films. These include amorphous, small crystallites in an amorphous matrix, polycrystalline, small grain epitaxial, large grain epitaxial with low angle intragranular boundaries, and monocrystalline. Typical examples of each type of film are contained in
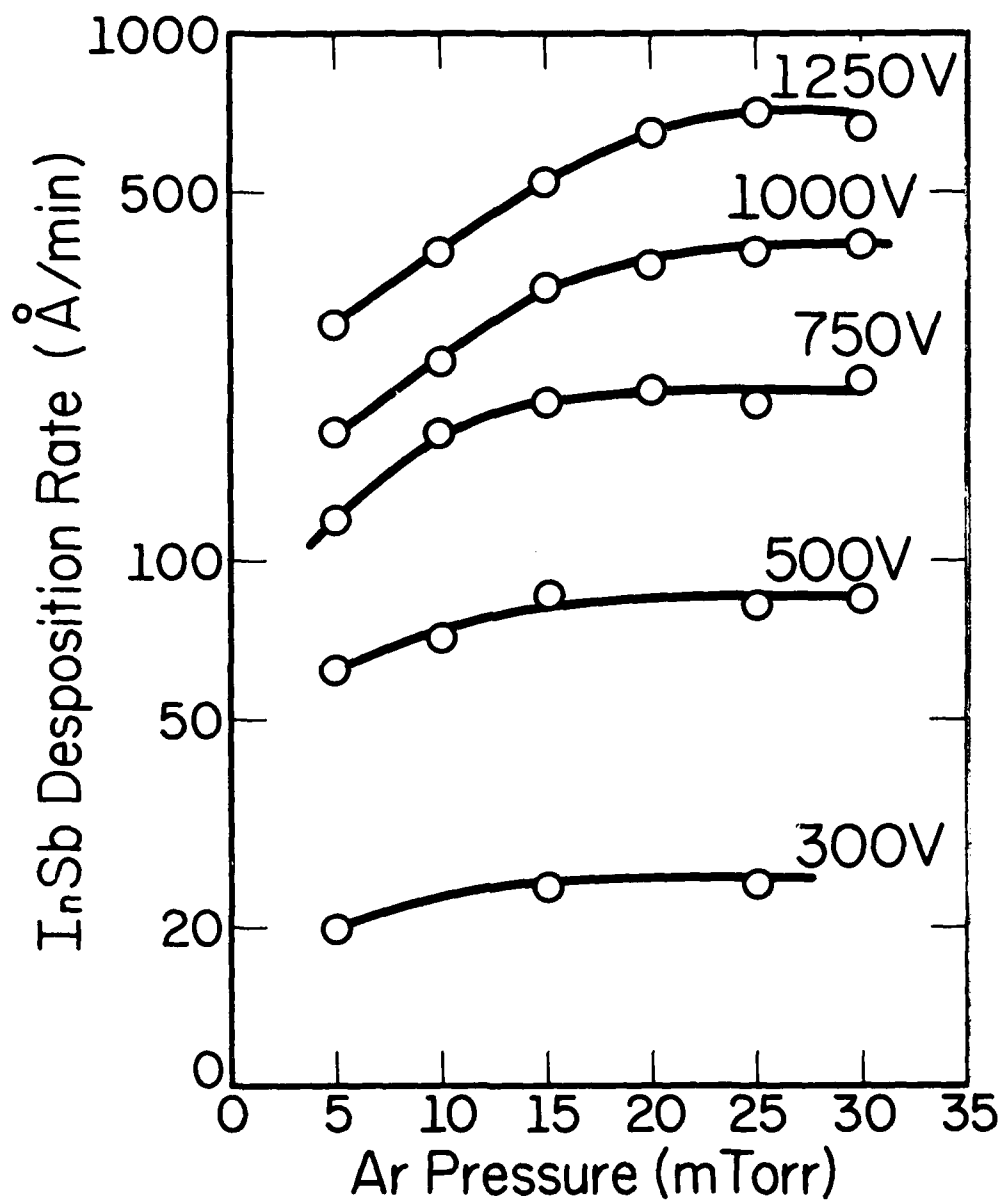
Figure 4. The deposition rate of InSb as a function of Ar sputtering pressure for various target biases.
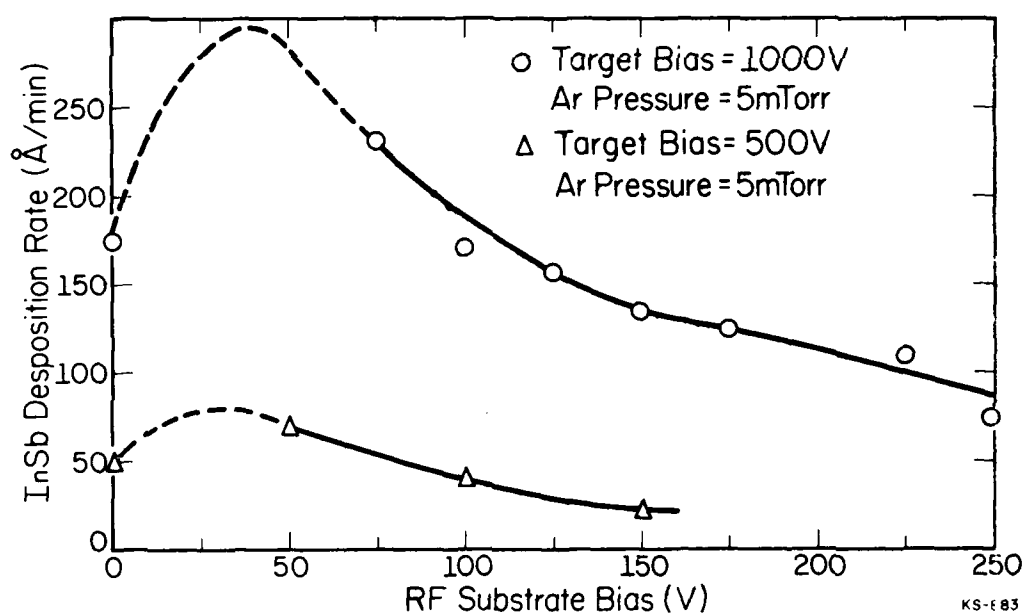
KS-8.84

Figure 5. The deposition rate of InSb as a function of applied RF substrate bias for target biases of 1000 V and 500 V at 5 mTorr.

this section. All micrographs shown were taken from 1800 $\overset{o}{A}$ thick films grown with an argon sputtering pressure of 5×10^{-3} Torr.

Figure 6a is a micrograph of an amorphous InSb film sputter deposited on p-a CaF_2 using a deposition rate of 100 $\overset{o}{A}$/min and a substrate temperature of $50^{o}C$. The triangular regions in the micrograph are replicas of thermal annealing pits which form on the CaF_2 surface during the high temperature vacuum anneal. The microstructure of a large grain epitaxial film with low angle intragranular boundaries is presented in Figure 6b. This film was grown at $400^{o}C$ using a deposition rate of 100 $\overset{o}{A}$/min. The selected area diffraction pattern in Figure 6b is from the dark area in the upper right-hand corner of the micrograph.

A plot of the average grain size of InSb films grown on p-a CaF_2 as a function of growth conditions is given in Figure 7 in which the measured grain size has been normalized to the film thickness. This was done since we observed, in agreement with Williamson[16] who investigated evaporated InSb, that the average grain size is strongly dependent on the film thickness. All films investigated were between 1000 $\overset{o}{A}$ and 2000 $\overset{o}{A}$ thick. In general the average grain size of RF sputtered InSb on p-a CaF_2 can be increased by decreasing the deposition rate or by increasing the substrate temperature.

Figure 8 summarizes the TEM results for InSb films deposited on p-a CaF_2 with various deposition rates and substrate temperatures. The polycrystalline to epitaxial transition temperature was slightly rate dependent and increased from approximately $200^{o}C$ to $350^{o}C$ as the deposition

Figure 6a.   An Electron micrograph of RF sputter deposited
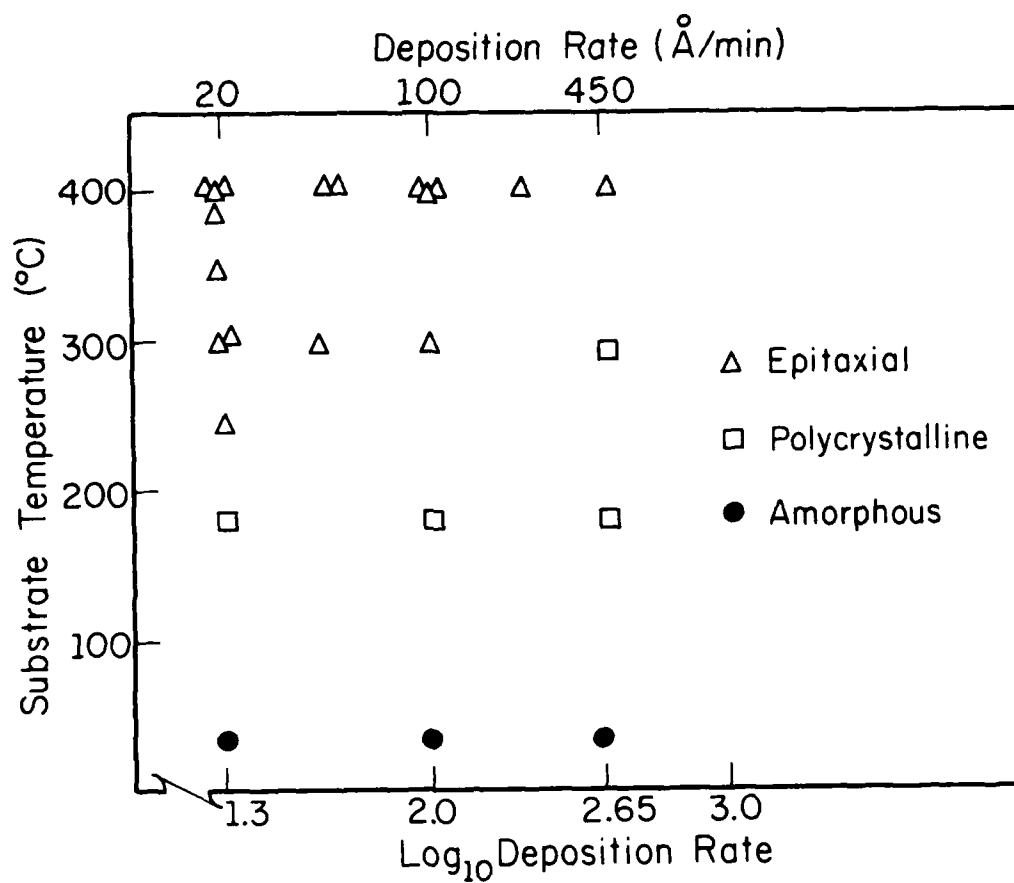   InSb grown on a p-a CaF_2 substrate at 50°C.

Figure 6b. An electron micrograph of RF sputter deposited
InSb grown on a p-a CaF_2 substrate at 400°C.
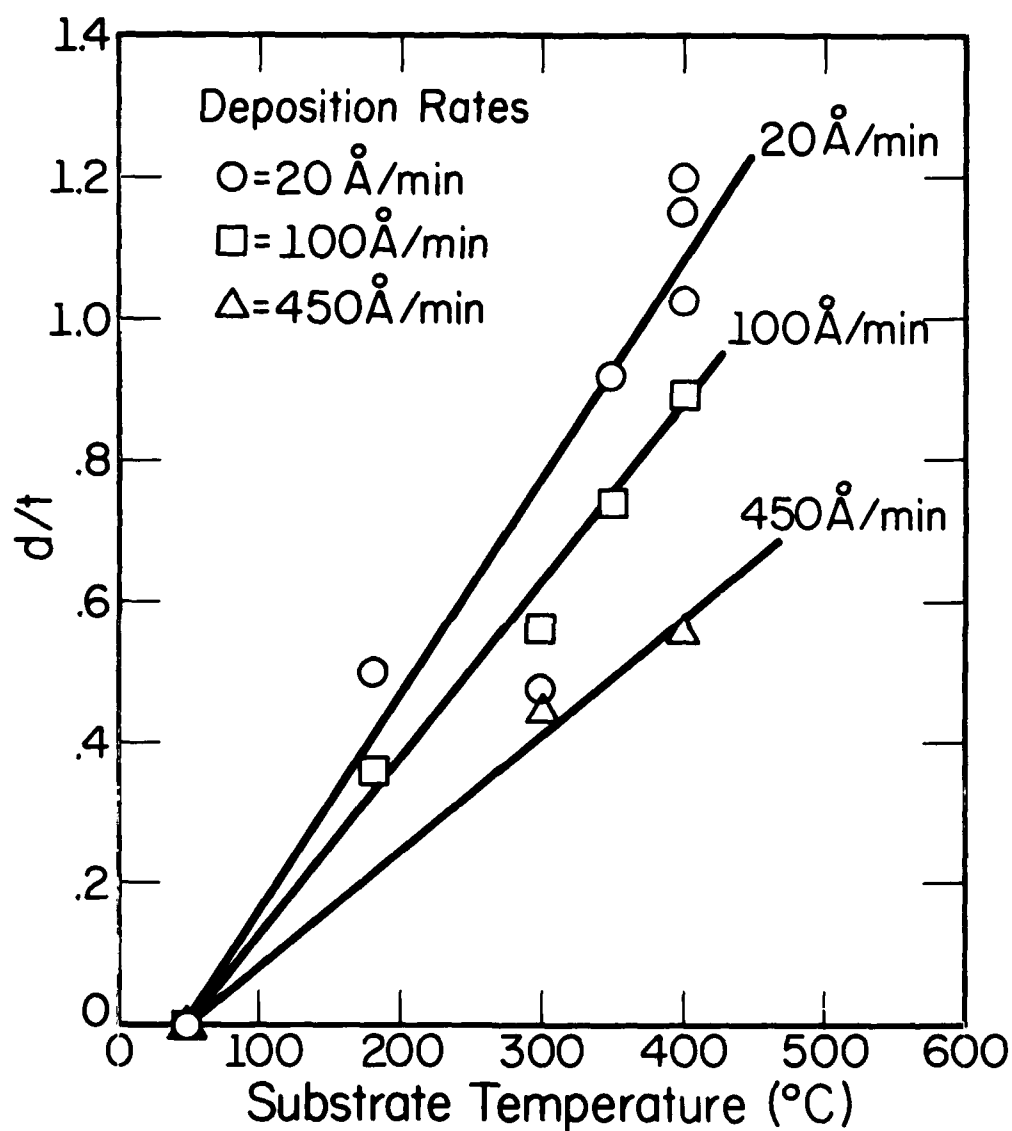
Figure 7. The normalized grain size of RF sputter deposited
InSb grown on p-a CaF_2 substrates as a function of
substrate temperature for deposition rates of
20 Å/min, 100 Å/min, and 450 Å/min.

Figure 8. The microstructure of RF sputter deposited InSb grown on p-a CaF$_2$ as a function of deposition rate.

KP-972

rate increased from 20 Å/min to 450 Å/min. However, for all deposition rates, crystalline films were observed when the substrate temperature was 180°C or higher.

A slight decrease in the polycrystalline to epitaxial transition temperature occurred when cleaved CaF_2 substrates were used. Figure 9a shows the microstructure of an InSb film sputter deposited on cleaved CaF_2 at 30°C with a deposition rate of 20 Å/min. In this case the microstructure may be classified as small crystallites in an amorphous matrix. InSb sputtered on cleaved CaF_2 at 400°C is small grained polycrystalline as shown in Figure 9b. The lines at the top and bottom of the micrograph are due to replication of cleavage steps on the (111) CaF_2 surface. From the preferred orientation in the diffraction pattern and the fact that the cleavage steps must be in ⟨110⟩ directions, the epitaxial relationship between RF sputter deposited InSb and cleaved CaF_2 has been determined to be;

$$(111)_{InSb} \parallel (111)_{CaF_2}$$

and

$$[1\bar{1}0]_{InSb} \parallel [1\bar{1}0]_{CaF_2}$$

An electron micrograph of an InSb film grown on a p-a CaF_2 substrate is shown in Figure 9c. The film was grown under the same conditions as the film in Figure 9b, and yet shows a much lower degree of preferred orientation. However, the grain size was found to be larger in the film grown on the p-a CaF_2 substrate. This effect of decreased grain size and increased texture when cleaved surfaces were used occurred quite generally
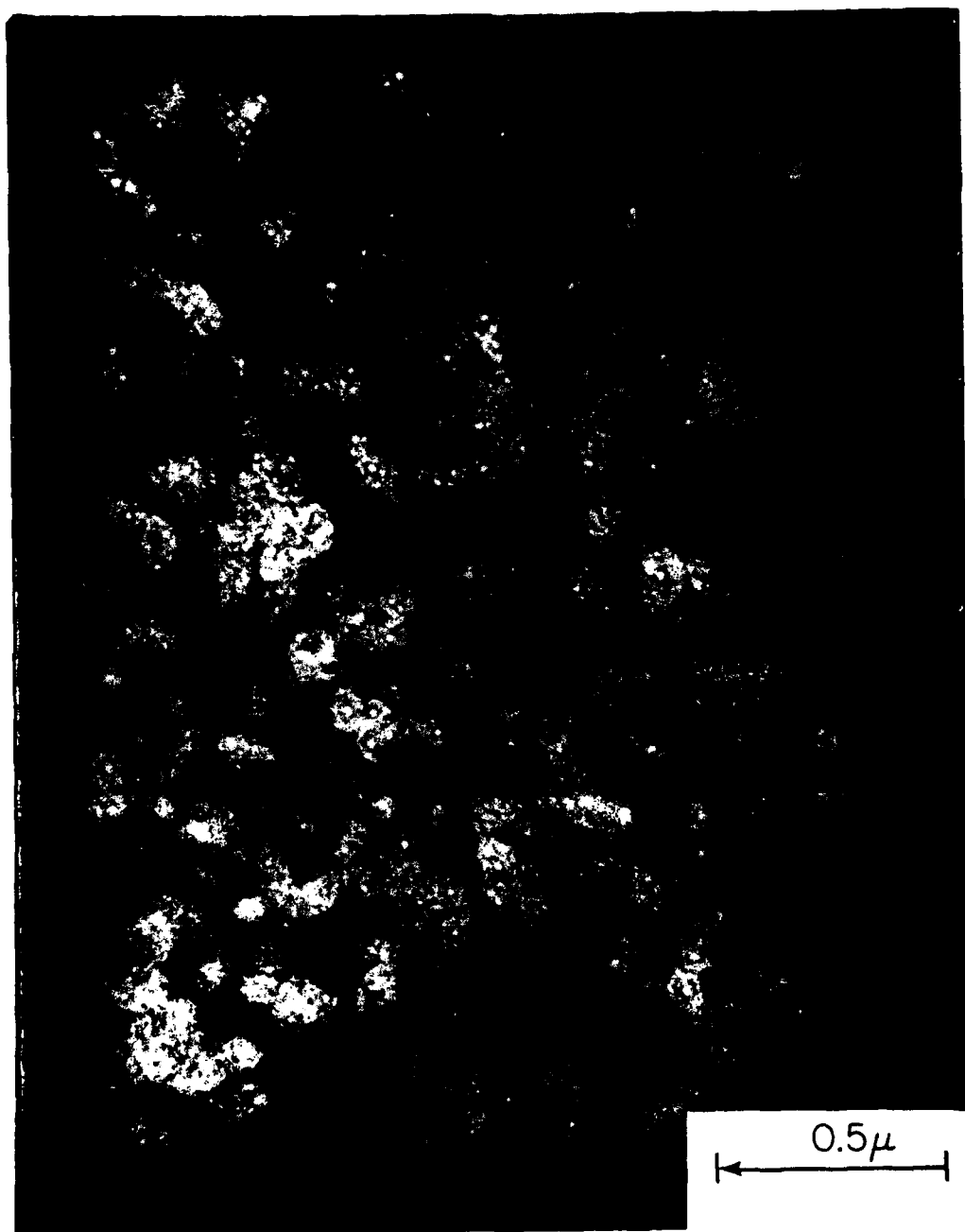
0.5μ

Figure 9a. Electron micrograph of InSb films RF sputter
deposited at a rate of 20 Å/min on cleaved
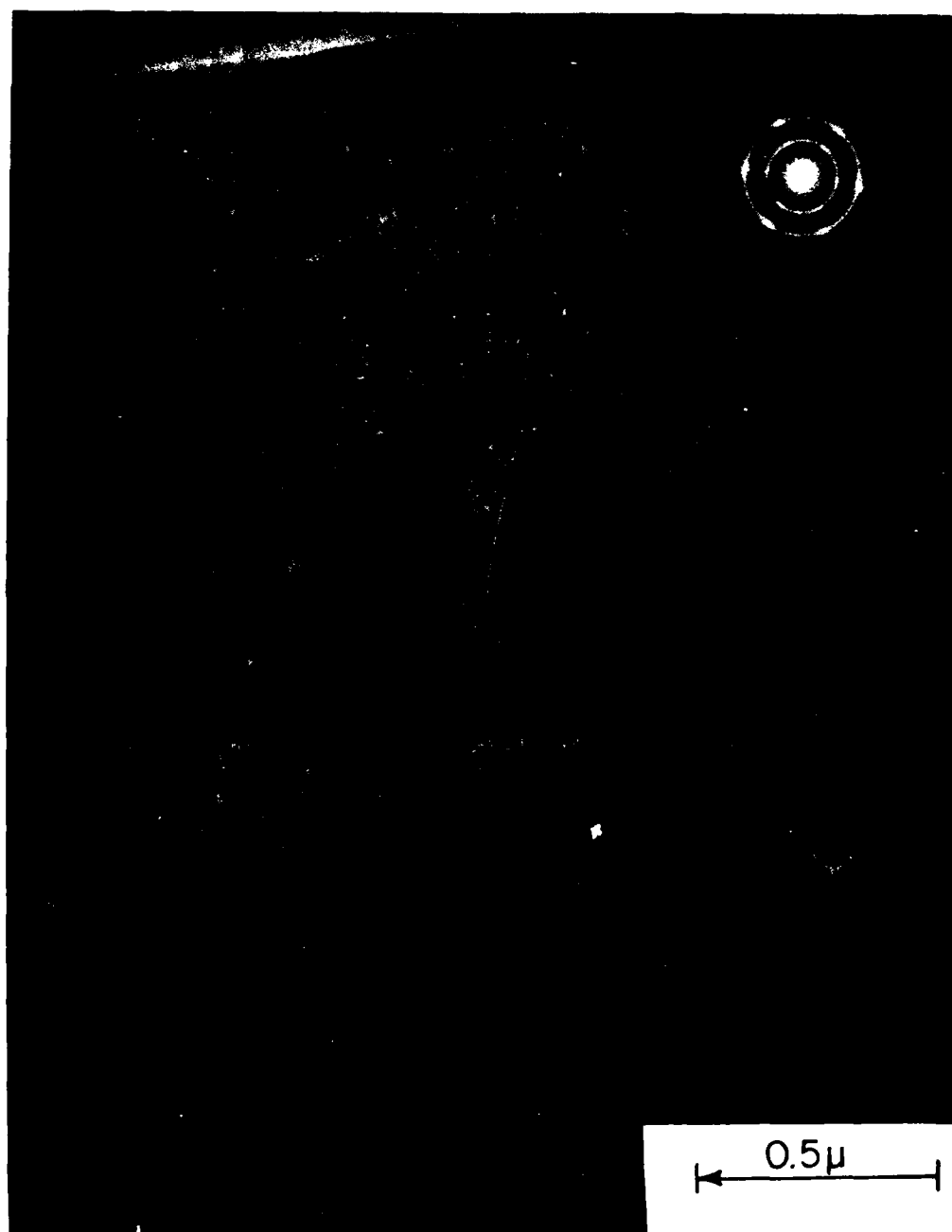CaF₂ at 30°C.

0.5μ

Figure 9b.   Electron micrograph of InSb films RF sputter
             deposited at a rate of 20 Å/min on cleaved CaF$_2$
             at 400°C.

Figure 9c. Electron micrograph of InSb films RF sputter
deposited at a rate of 20 Å/min on p-a CaF_2
at $400°C$.

for both CaF_2 and BaF_2 substrates.

Figures 10a and 10b are electron micrographs of InSb films grown on cleaved NaCl at a substrate temperature of 50°C and 400°C respectively. The deposition rate in both cases was 20 Å/min. A strong $(100)_{InSb} \parallel (100)_{NaCl}$ epitaxial relationship is apparent. The grain size is, however, again quite small when compared with films grown on p-a CaF_2. Films grown on NaI also showed a strong $(100)_{InSb} \parallel (100)_{NaI}$ epitaxial relationship at 400°C, but the rapid attack of the NaI surface by water vapor makes NaI a poor substrate for reproducible experimentation.

Monocrystalline InSb was grown on cleaved BaF_2 at substrate temperatures as low as 180°C with a deposition rate of 20 Å/min as shown in Figure 11. The epitaxial relationship between film and substrate is again

$$(111)_{InSb} \parallel (111)_{BaF_2}$$

and

$$[1\bar{1}0]_{InSb} \parallel [1\bar{1}0]_{BaF_2}$$

Figure 12 summarizes the electron diffraction and microstructure data as a function of substrate material and substrate temperature for RF sputtered InSb films. All results shown in Figure 12 are for a deposition rate of 20 Å/min. A general trend of increasing amount of preferred orientation with increasing lattice mismatch appears at elevated temperatures. The surface damage caused by water vapor attack of NaI results in a reduction in the quality of films deposited on these substrates.

0.5µ

Figure 10a. Electron micrograph of InSb RF sputter deposited on cleaved NaCl with a deposition rate of 20 Å/min at 50°C.
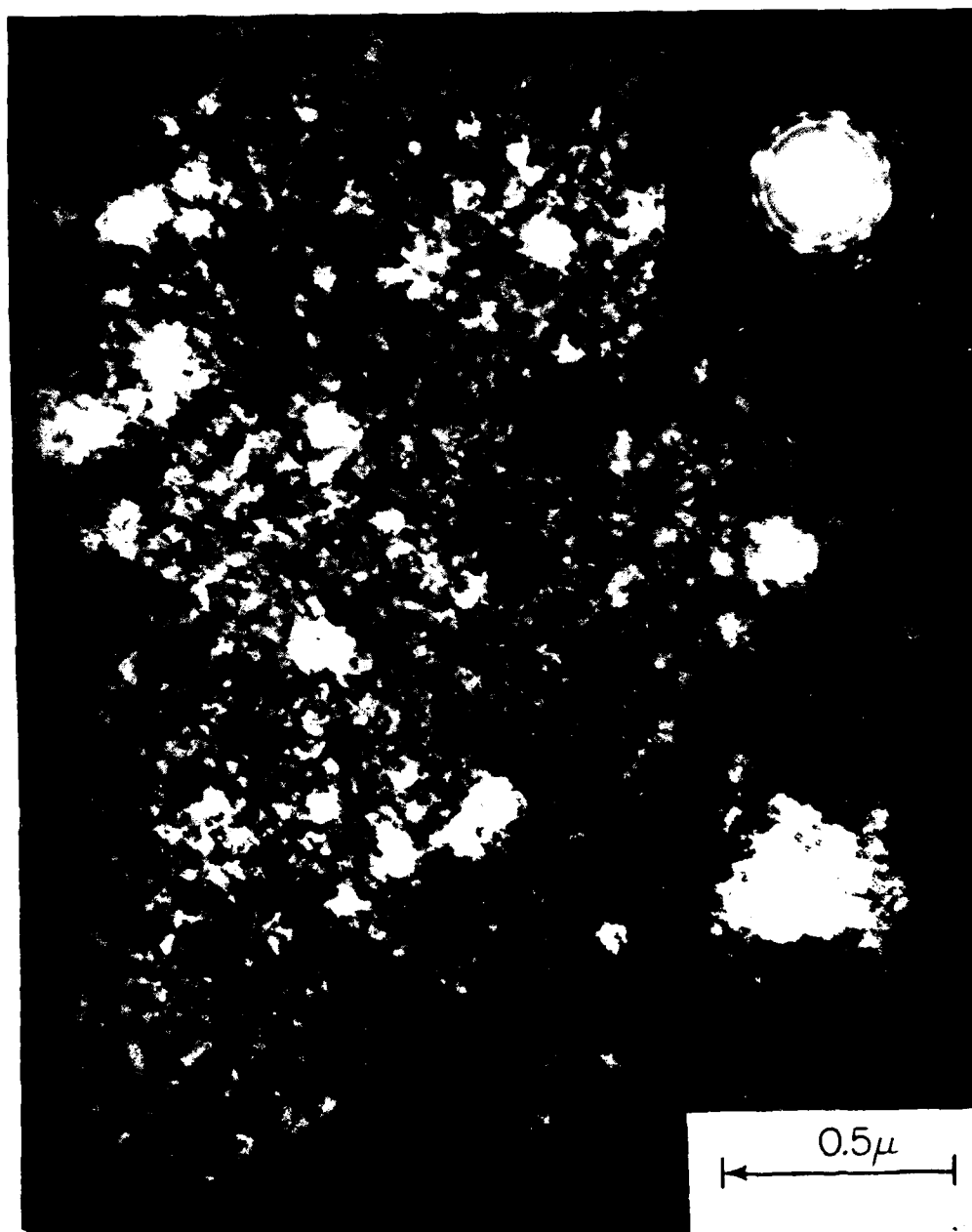
Figure 10b. Electron micrograph of InSb RF sputter deposited on cleaved NaCl with a deposition rate of 20 Å/min at 400°C.

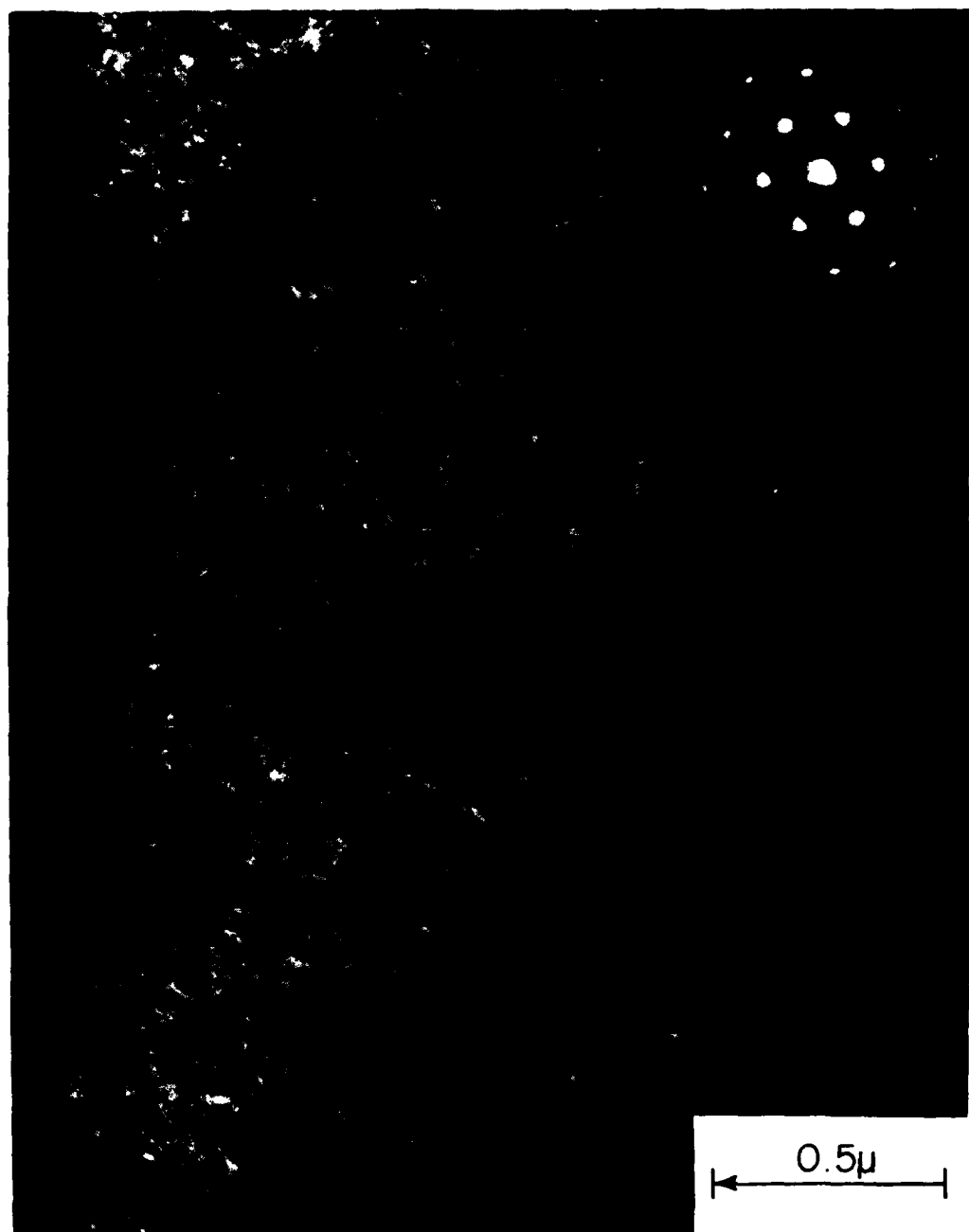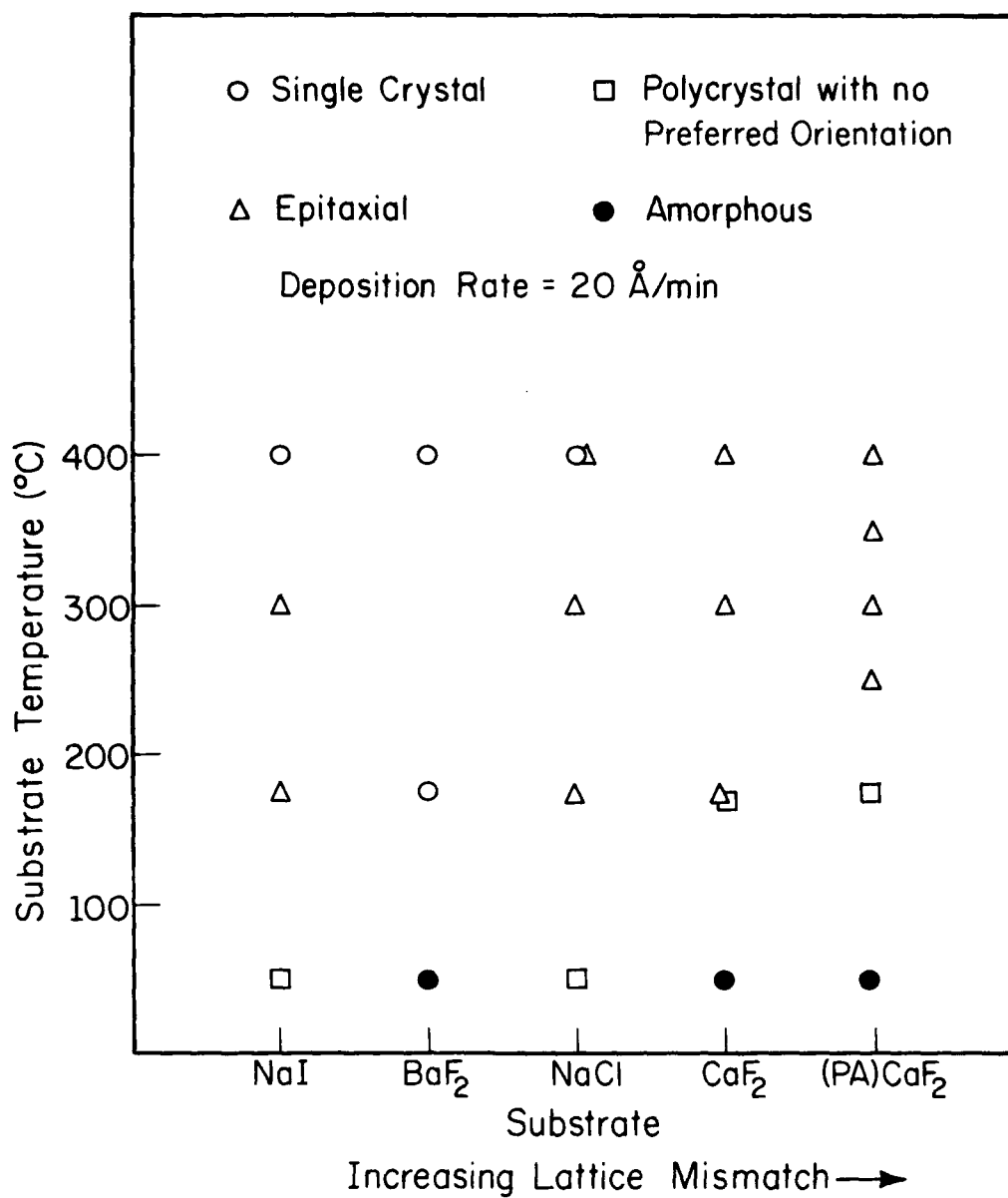Figure 11. Electron micrograph of InSb deposited on cleaved
BaF$_2$ at 180°C with a deposition rate of 20 Å/min.

Figure 12.   The microstructure RF sputter deposited InSb as a
function of substrate material and growth temperature.

IV.C. Chemical Analysis

Auger electron spectra were taken of the films used for electrical measurements. Chemical concentration was determined by comparing the peak-to-peak differentiated elemental intensities obtained from the films to those of a bulk standard. The MNN 404 eV indium and 454 eV antimony lines were used since these lines showed no energy shifts or changes in line shape from sample to sample. The estimated accuracy of this technique is $\pm$ 5%. The In/Sb ratios for films grown at substrate temperatures below 300°C were always found to be unity within experimental error. However, films grown at 400°C consistently showed an antimony deficiency. Figure 13 shows typical Auger spectra from a bulk InSb sample and a film grown at 400°C with a deposition rate of 20 Å/min.

Electron diffraction results revealed the presence of free indium and indium oxide in samples grown at 400°C on NaCl and NaI substrates. Both the indium and indium oxide disappeared when the film was rinsed in HCl acid indicating that these impurities are present at one or both of the film surfaces.

IV.D. Electrical Measurements

Electrical measurements were made on films grown on p-a CaF_2. These substrates were used in order to eliminate carrier scattering from cleavage steps. CaF_2 also has the advantage that it is not hygroscopic. All films used in this part of the investigation were approximately 1800 Å thick. This thickness was chosen as a compromise between thinner films in which surface scattering dominates and thicker films which exhibit
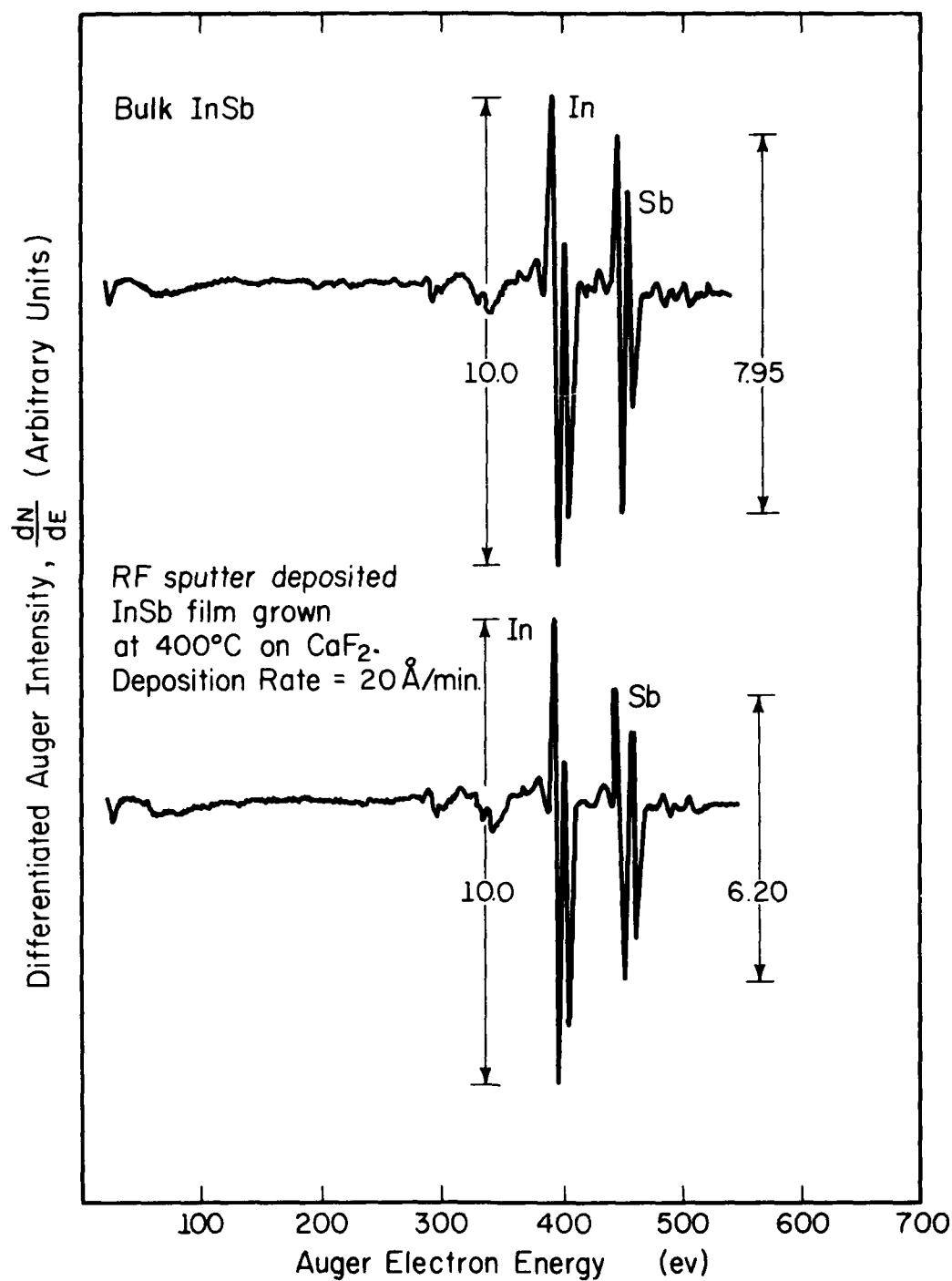
Figure 13. A comparison between the Auger electron spectra
obtained from bulk InSb and an RF sputtered InSb
thin film grown on p-a CaF_2 at 400°C and 20 Å/min.

large differential thermal expansion stresses sometimes causing spontaneous film delamination. Hall mobilities and net carrier concentrations were determined from Hall coefficient and van der Pauw resistivity measurements. All films were found to be n-type with net carrier concentrations in the range of 10^{17} cm^{-3}.

Lou and Epstein[19] have shown that a depletion layer is formed when InSb is flash evaporated onto CaF_2 single crystals. They measured the depth of charge depletion by determining the conductance per unit area of the film as a function of the film thickness. The depletion depth was found to obey the relation;

$$GL/w = \sigma(t - 2d_o) \qquad (4.2)$$

where G is the conductance of the film; L, w, and t are the length, width, and thickness of the sample respectively; and σ is the conductivity of the film which is determined by the slope of a plot of GL/w as a function of thickness. The intercept of the curve with the film thickness axis gives the total depletion depth. For van der Pauw resistivity measurements equation 4.2 becomes

$$t/\rho_m = \sigma(t - 2d_o) \qquad (4.3)$$

where ρ_m is the measured resistivity. A plot of t/ρ_m as a function of film thickness is given for our samples in Figure 14. The equivalent depletion depth is independent of the growth conditions. For InSb RF sputtered onto p-a CaF_2, the value of $2d_o$ is approximately 1000 Å.
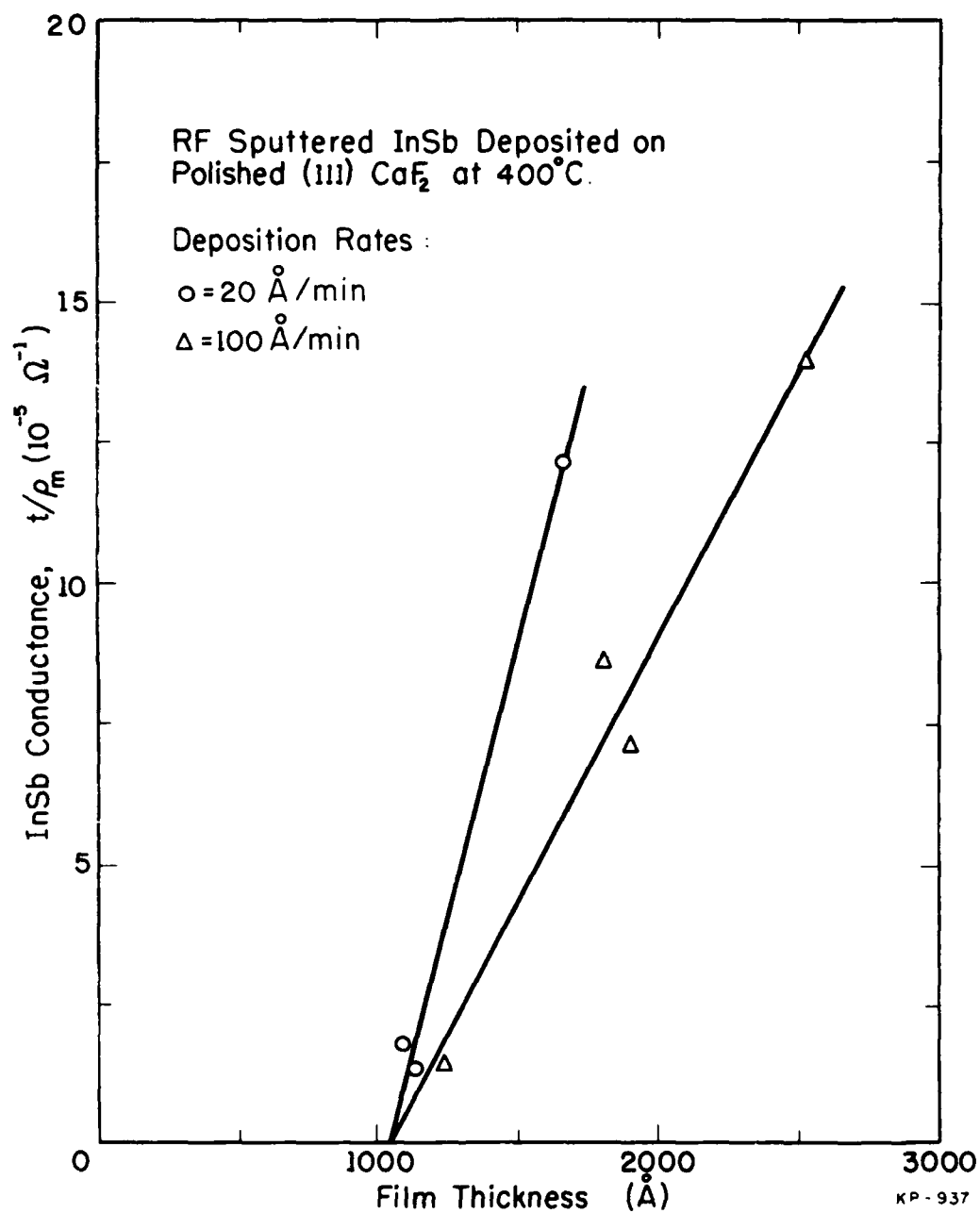
Figure 14. A plot of conductance as a function of film thickness for InSb deposited on p-a CaF$_2$ at 400°.

Figure 15 is a plot of the Hall mobility and the net carrier concentration as a function of deposition temperature. A slight reduction in the net carrier concentration occurs as the substrate temperature is raised. The electron mobility increases with increasing substrate temperature and appears to be relatively insensitive to the deposition rate. Figure 16 shows the net carrier concentration and conductivity of a film grown on p-a CaF_2 at 400°C with a deposition rate of 100 Å/min. The slope of the conductivity curve at room temperature gives an electrical band gap of 0.21 eV, which is in good agreement with the results of other workers.[10] The measured electron mobility as a function of reciprocal temperature is given in Figure 17.

IV.E. The Effects of RF Substrate Biasing

The etch rate of CaF_2 at 20 mTorr is 0.22 Å/V-min. However, RF sputter etching appears to have an adverse effect on the metallurgical properties of RF sputter deposited InSb thin films. The results are summarized in Table 3.

Application of an RF bias to the substrate during film growth caused a reduction in the amount of preferred orientation observed in the films and also a reduction in the net carrier concentration. The reduction in the amount of preferred orientation with applied RF substrate bias occurred in films deposited on both cleaved and p-a substrates. An example of the reduction in preferred orientation is given in Figure 18.
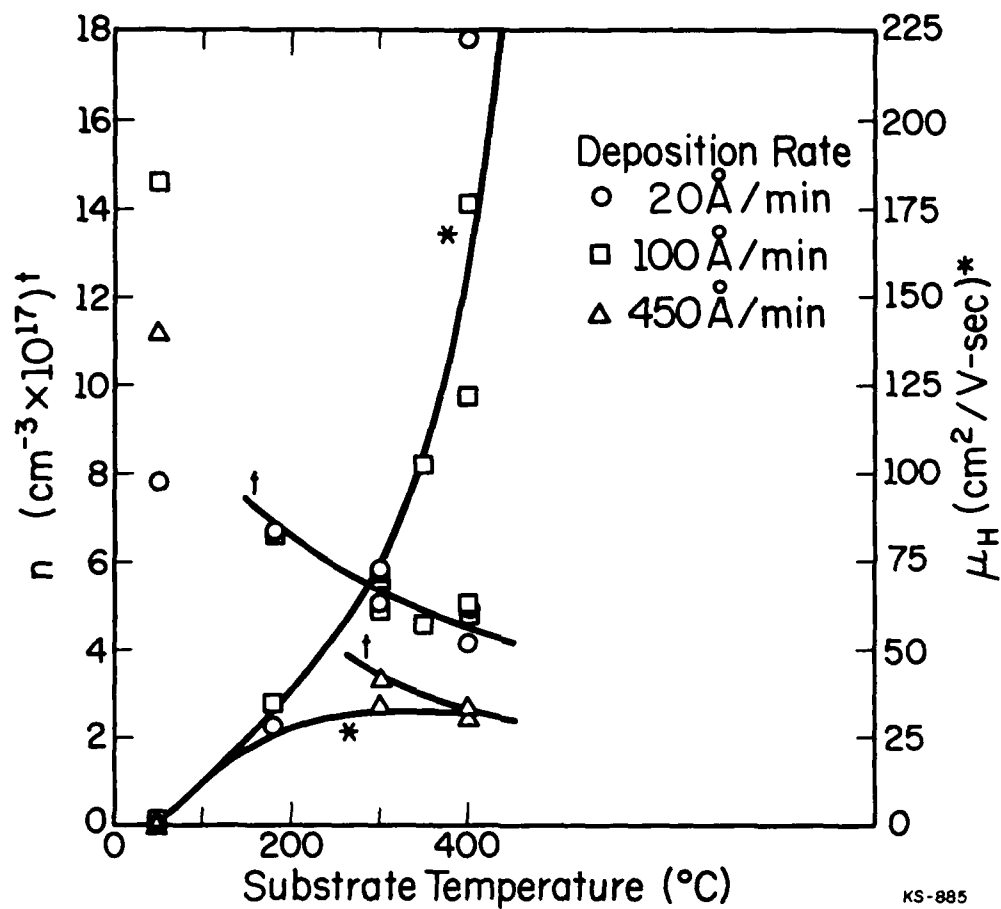
Figure 15. The room temperature electron mobility and net
carrier concentration of RF sputter deposited
polycrystalline InSb on p-a CaF$_2$ as a function
of growth temperature.
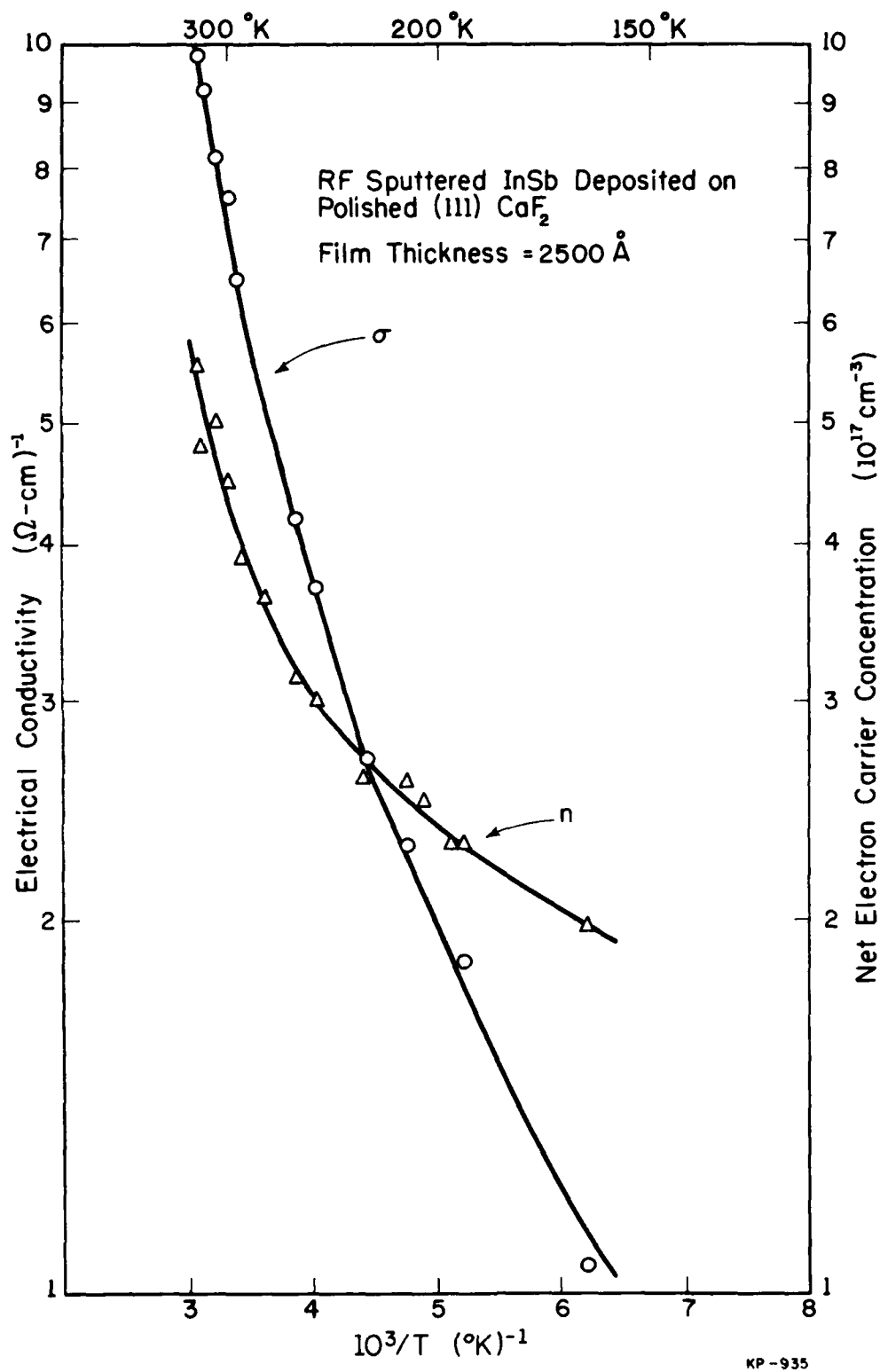
Figure 16. The temperature dependence of the net carrier concentration and electrical conductivity of a 2500 Å thick InSb film RF sputter deposited on p-a CaF$_2$ at 400°C.
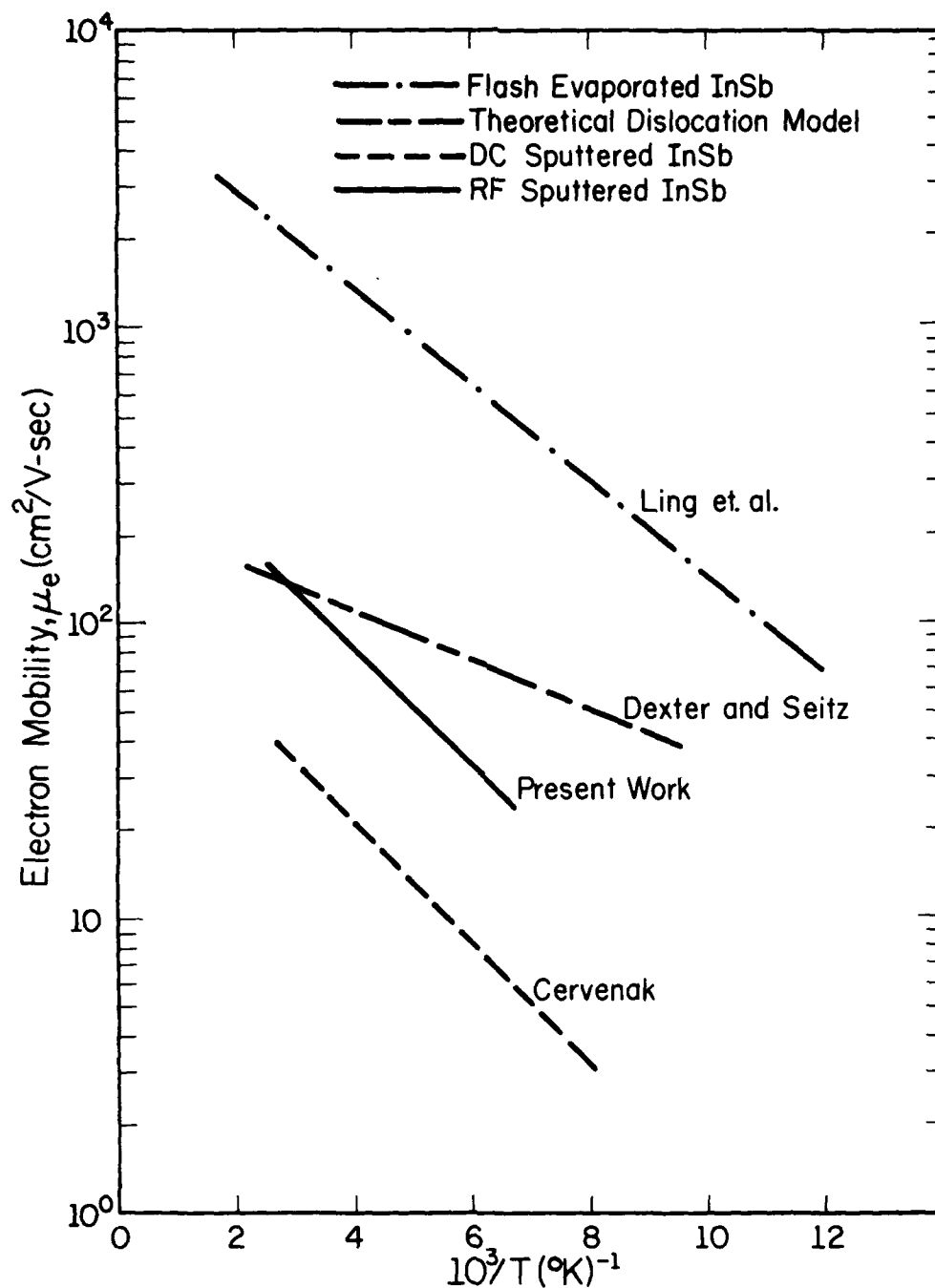
Figure 17. The measured temperature dependence of the electron mobility of polycrystalline RF sputter deposited InSb grown at 400°C compared with InSb electron mobilities reported by Cervenak[7] and Ling et. al.[8] as well as the theoretical temperature dependence of mobility proposed by Dexter and Seitz.[27]

TABLE 3

The Effect of Substrate Bias on the Properties of
InSb Films Sputter Deposited on p-a CaF$_2$ at 400°C

Run #	Target Bias (V)	Substrate Bias (V)	Deposition Rate (Å/min)	Etch Bias (V)	Thickness CaF$_2$ Removed (Å)	Crystallinity	Electron Mobility (cm2/V-sec)	Net Carrier Concentration (x10^{17} cm^{-3})
5	-300	-	20	-	-	Epitaxial	200	5.4
6	-750	-	92	-	-	Epitaxial	12₊	5.6
26	-300	-	20	-500	1100	Polycrystal	24.2	2.6
27	-300	-	20	-250	550	Polycrystal	36.9	4.6
37	-750	-100	71	-100	100	Polycrystal	27.5	4.7
43	-300	-25	20	-25	50	Epitaxial	47.1	1.0

Figure 18a is an electron diffraction pattern of an InSb film grown on a
cleaved NaI substrate at 400°C without an applied RF substrate bias, while
Figure 18b is an electron diffraction pattern of an InSb film grown
under identical conditions except that an RF substrate bias of 25 V was
applied during growth. The magnitude of the bias was chosen so that the
deposition rate was maintained constant at 20 $\overset{o}{A}$/min.

The observed reduction in net carrier concentration with bias could be
due to a combination of several effects such as the introduction of p-type
impurities or lattice defects into the film due to ion bombardment or the
preferential resputtering of n-type impurities. In addition, the application
of the RF substrate bias during film growth eliminates the thin surface
layers of indium and indium oxide which we believe form at the film-substrate
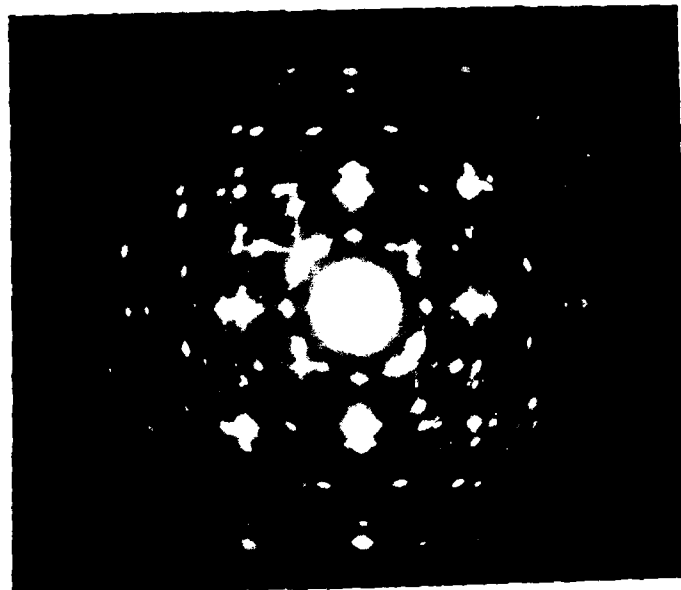interface.

Figure 18. Electron diffraction patterns of InSb RF sputter deposited on cleaved NaI substrates (a) with no externally applied substrate bias and (b) with an applied bias of -25 V.

V. DISCUSSION

Deposition rate, substrate material, substrate preparation, and growth temperature are important interdependent variables which determine the sputtered film structure. The deposition rate and its relation to substrate temperature, sputtering pressure, and RF substrate bias will be discussed in the first section of this chapter. The second section contains a discussion of the effects of varying the substrate material, substrate preparation, and growth temperature on the structure and electrical properties of sputtered films. Possible electron mobility limiting mechanisms will be presented in the final section and the dominant charge scattering mechanism will be identified.

V.A. Deposition Rate

Figures 3, 4, and 5 show that the measured InSb deposition rate depends primarily on the target voltage and the sputtering pressure, and to a lesser extent on the substrate temperature and substrate bias. Equation 4.1 is an empirical relationship between the measured deposition rate and the target voltage in which the rate coefficient, R_o, is a function of both the sputtering pressure and the substrate temperature. From the data presented in Table 2, R_o can be expressed as

$$R_o = g - h(T_s - T_o) \tag{5.1}$$

where g and h are constants which depend on pressure and T_o is the substrate temperature prior to deposition.

During film deposition the substrate temperatue increases due primarily to bombardment of the substrate by energetic secondary electrons originating at the target and to plasma radiation.[20] From Figure 1, the

temperature increase can be written as

$$T_s = T_f - (T_f - T_o) \exp(-\alpha t) \tag{5.2}$$

where T_f is the final steady state deposition temperature and α is the thermal time constant of the substrate. Substitution of equations 5.1 and 5.2 into equation 4.2 gives an expression for the time dependent deposition rate which decreases exponentially until a steady state rate, R_f, is reached. R_f is a function of the power input into the plasma, plasma geometry, secondary electron yield of the target, and the reflectivity of the deposited film.

The measured deposition rate, R_m, is the time average of the instantaneous deposition rate which can be found by combining equations 4.1, 5.1, and 5.2 and integrating over the elapsed sputtering time. The measured deposition rate is then

$$R_m = \left[g - h(T_f - T_o) - h(T_f - T_o) \left(\frac{1 - \exp(-\alpha t)}{\alpha t} \right) \right] (V - V_c)^b \tag{5.3}$$

The initial deposition rate, R_i, can be found by setting t equal to zero and T_f equal to T_o. The relative difference between R_m and R_i is then

$$\frac{R_i - R_m}{R_i} = \frac{h(T_f - T_o)}{g} \left[\frac{(1 - \exp(-\alpha t))}{\alpha t} - 1 \right] . \tag{5.4}$$

In the present experiments the largest difference between the measured deposition rate and the initial deposition rate was approximately 25 Å/min for a target bias of 1800 V. Comparing this difference with the measured deposition rate at 1800 V gives a relative difference of only 5.5% which is less than the measurement accuracy for R_m. Therefore, in this thesis deposition temperature and deposition rate are reported as T_i and R_m respectively. The

above analysis can be used as an indirect measure of plasma heating

effects at the substrate provided that the relative difference between the

initial and measured deposition rates is larger than the experimental

uncertainty.

Figure 4 shows that for low pressures at constant target bias

the measured deposition rate increases with pressure. This is because the

ion density in the plasma increases with pressure. However, as the pressure

is further increased a saturation region is reached. This saturation

region occurs when the mean free path of the argon ions becomes less than

the cathode fall distance. The reduction in mean free path causes a decrease

in the average energy of the particles striking the target and hence a

reduction in sputtering yield. These two effects, the increase in ion

density and the decrease in sputtering yield, balance to give a constant

sputtering rate. The onset of saturation shifts to higher pressures as the

target bias is increased. This is due to the fact that the yield increases

faster than the ion density with an increase in the applied target bias,

and hence a higher pressure is required to reach saturation.

As we have shown in Figure 5, RF substrate biasing affects the

deposition rate. Cuomo et. al.[18] have proposed a model for determining

the deposition rate as a function of RF bias. They assumed that the

reduction in deposition rate at high RF substrate bias was due to resputtering

of the film or in other words, a reduction in the sticking coefficient of the

incident atoms. The increased deposition rate at small RF substrate biases

is caused by an increase in the net plasma ionization due to an increased

secondary electron yield at the substrate. Using this physical model,

Cuomo et. al. derived the following relationship between the normalized deposition rate (A_n) and the externally applied substrate bias (V_b),

$$A_n = (1 + m_n V_b^p)\left(1 - \frac{(V_b^{\frac{1}{2}})(V_b - V_c)^{\frac{1}{2}}}{(V_f^{\frac{1}{2}})(V_f - V_c)^{\frac{1}{2}}}\right) \qquad (5.5)$$

where m_n is a constant related to the maximum value of A_n, V_f is the value of the substrate bias when the deposition rate goes to zero, and p is a constant which depends on the material being deposited. The general form of the curves in Figure 5 agrees with equation 5.5.

V.B. *Film Structure*

The normalized grain size of thin films generally increases with increasing substrate temperature and decreases with increasing deposition rate. This dependence of grain size on the substrate temperature and deposition rate has been reported for many different thin film growth techniques,[21] and is related to the increased surface mobility of deposited atoms as well as bulk annealing effects. Figure 7 shows that RF sputtered polycrystalline InSb films follow this general trend.

In Figures 8 and 12 the dependence of the epitaxial temperature on substrate material and deposition rate can be seen. Substrate material influences the epitaxial temperature in two ways. An increase in the lattice mismatch between the deposited film and the substrate tends to increase the epitaxial temperature, while surface contamination can increase or decrease the epitaxial temperature depending on the type of

contamination and the nucleation kinetics. The effect of lattice mismatch can be seen in Figure 12 where the epitaxial temperature of InSb is reduced at least $120^{\circ}C$ when cleaved BaF_2 substrates (M = 4.35%) are substituted for cleaved CaF_2 substrates (M = 18.5%). The dependence of epitaxial temperature on the deposition rate can be seen in Figure 8. Increasing the deposition rate from 20 $\overset{o}{A}$/min to 450 $\overset{o}{A}$/min increases the epitaxial temperature by at least $50^{\circ}C$. The increase in the epitaxial temperature with increased sputtering rate is related to a decrease in the surface mobility of the deposited atoms. Krikorian and Sneed[12] have also observed this effect in DC sputter deposited germanium films.

The effect of surface preparation on film quality can be seen by comparing the epitaxial temperature and grain size of InSb films deposited on cleaved CaF_2 and p-a CaF_2 substrates. At constant temperature the amount of preferred orientation in films deposited on cleaved CaF_2 was in all cases greater than the amount of preferred orientation in films deposited on p-a CaF_2 substrates. However, the grain size of films grown on p-a CaF_2 substrates was consistently larger than the grain size of films deposited on cleaved substrates. The first of these effects appears to be due to the growth of a thin contaminated layer at the p-a CaF_2 surface during the anneal. Auger depth analysis revealed a high oxygen content at the InSb-CaF_2 interface and Wickersham and Hanking[22] have reported the formation of $CaCO_3$, CaO, and $Ca(OH)_2$ upon annealing CaF_2. This contaminated layer would tend to inhibit epitaxial growth. The small grain size observed in films grown on cleaved CaF_2 is due to the large amount of preferred orientation which limits grain growth during annealing.

Surface states at both the film-atmosphere and film-substrate interfaces are responsible for the depleted layers discussed in section IV.D. The depleted layers do not take part in the conduction processes to the same extent as the non-depleted regions. Therefore the measured conductivity and net carrier concentrations must be corrected for this effect which reduces the effective film thickness by approximately 1000 Å as determined from Figure 14. However, it is not necessary to correct measured mobility values since the thickness terms in the conductivity and the net carrier concentration cancel.

A reduction in the net carrier concentration with increasing annealing temperature similar to the data given in Figure 15 has been reported in bulk n-type InSb by several investigators.[23,24] Dzhanelidze and Kurdiani[23] have measured the evaporation rates of indium and antimony for bulk InSb at a pressure of 10^{-4} Torr and they reported that the maximum ratio of antimony to indium loss was approximately 4 and it occurred at a temperature of $400^{\circ}C$. This antimony deficiency appears to be related to the decrease in the electron carrier concentration. The results of Auger electron spectroscopy and electron diffraction measurements indicate a deficiency of antimony in InSb films grown above $300^{\circ}C$. However, from physical chemistry arguments antimony vacancies should act as donors rather than acceptors.

Recent work by Chiang and Pearson[25] with GaAs indicates that the diffusion coefficient of the group V vacancy is much less than the diffusion coefficient of the group III vacancy. Therefore, at elevated temperatures the group III vacancy, which acts as an acceptor, can diffuse throughout the film while the group V vacancy, which acts as a donor, remains near the surface in the depletion region. Since the InSb film is strongly depleted,

the electrical measurements yield information only on the internal non-depleted regions of the film. Combining this fact with the results of Chiang and Pearson, the decrease in net carrier concentration with increased substrate temperature can be satisfactorily explained by a net diffusion of p-type indium vacancies into the non-depleted n-type regions of the film causing a reduction in the measured electron carrier concentration.

V.C. Electron Mobility and Scattering Mechanisms

The identification of the primary scattering mechanism in the films is essential for a complete understanding of the electrical properties of the films. In general the electron mobility is given by

$$1/\mu = 1/\mu_i + 1/\mu_p + 1/\mu_s + 1/\mu_d + 1/\mu_{pb} \tag{5.6}$$

where μ_i and μ_p are limited by impurity and phonon scattering respectively, μ_s is due to surface scattering, μ_d is due to scattering by edge dislocations present in the film, and μ_{pb} is due to scattering at potential barriers which arise from the electric field associated with the pile up of dislocations.

The magnitude of the measured electron mobilities in the films is much too low for impurity scattering or phonon scattering to have an appreciable effect. Surface scattering, however, could conceivably contribute significantly to the total scattering since the thickness of the films is only 2000 Å. The mobility due to surface scattering can be written as[26]

$$\mu_s/\mu_b = 1 - (2\lambda/(t - 2d_o))(1 - F(t,\lambda)) \tag{5.7}$$

where μ_b is the bulk mobility, which is 3×10^4 cm^2/V-sec at room temperature for samples with a net carrier concentration equivalent to that measured in the films, t is the film thickness, λ is the electron mean free path in the bulk crystal, and $F(t,\lambda)$ is a complicated function of t and λ which has been tabulated by Flietner.[26] For a 2000 Å InSb film with a 1000 Å depletion layer and a net carrier concentration of 3×10^{17} cm^{-3}, the mean free path for an electron is 2300 Å,[6] and the factor $F(t,\lambda)$ is 0.9. Using these values, equation 5.7 yields a value for the mobility of 15,000 cm^2/V-sec. Clearly this is much higher than the measured mobility and surface scattering can be neglected.

Dislocation scattering was first proposed by Dexter and Seitz[27] as a possible mobility limiting mechanism in semiconductors, and later this mechanism was used by Wieder[28] to explain the temperature dependence of the mobility of flash evaporated InSb thin films. Using the Dexter-Seitz model, Wieder showed that if the primary scattering centers were edge dislocations with their burgers vector in the plane of the film the mobility could be related to the dislocation density by

$$\mu_d = \frac{32}{3\pi} \left(\frac{1-v}{1-2v}\right)^2 \frac{KT\mathfrak{n}e}{e^2 Nmb^2} \tag{5.8}$$

where v is Poisson's ratio which is 0.33 for bulk InSb.[29] The energy associated with an edge dislocation, ϵ, is 6.4 eV[28] for InSb, and the magnitude of the burgers vector, b, is 4.6 Å for slip on (111) planes. N is the dislocation density. Using these values, the temperature dependence of dislocation scattering in InSb is given by

$$u_d = 8.9 \times 10^{11} (T/N) \ cm^2/V\text{-sec.} \qquad (5.9)$$

The dislocation density for a heteroepitaxial film can be calculated by a method suggested by Holt.[30] For an epitaxial (111) oriented InSb film on CaF_2, the calculated dislocation density is $2.8 \times 10^{12} \ cm^{-2}$. The actual dislocation density in the film should be slightly less than this amount since Holt's method does not take into account elastic deformation of the film. The logarithm of the mobility as a function of reciprocal temperature for a dislocation density of $2.4 \times 10^{12} \ cm^{-2}$ is given in Figure 17 assuming Dexter and Seitz's model. It should be noted that in this model the slope of the curve is independent of the dislocation density. A change in dislocation density will only affect the curve intercept if the Dexter-Seitz scattering mechanism is operative. Figure 17 also shows measured electron mobility data obtained from an RF sputtered InSb film grown at $400^{\circ}C$ with a deposition rate of 100 Å/min. Comparing the measured temperature dependence of the electron mobility with the theoretical dependence predicted using the Dexter and Seitz edge dislocation scattering model, it is clear that the dominant charge scattering mechanism is not due to isolated edge dislocations.

The potential barrier model was first proposed as a possible scattering mechanism in InSb by Gunther,[2] and later was used by Cervenak[7] and Ling et. al.[8] to describe the exponential behavior of the electron mobility with measurement temperature. They proposed that the primary scattering centers were the potential barriers associated with grain boundaries in the films. The relationship between the electron mobility and the measurement temperature in this model is given by

$$\mu_{pb} = (eu/kT)(\Sigma L/\Sigma N)\exp(-e\phi/kT) \qquad (5.10)$$

where $\Sigma L/\Sigma K$ is the mean distance between boundaries, e is the electron charge, u is the mean thermal velocity of the carriers, and ϕ is the potential barrier energy. Fitting our measured electron mobility data, which is given in Figure 17, to equation 5.10, a potential barrier energy of 0.04 eV is obtained. This value agrees with the values reported by Cervenak and Ling et.al.[6] for the potential barrier energies observed in DC sputtered and vacuum evaporated InSb films respectively. The results of Cervenak and Ling et. al. are also given in Figure 17.

The microstructure of a film grown at 400°C with a deposition rate of 100 Å/min is given in Figure 6b. This structure is characterized by large high angle grains with polygonized internal regions. The potential barrier scattering must be occurring at the intergranular polygonized boundaries, since the high angle boundaries are much too far apart to give the measured mobilities.

The potential barriers that appear at the boundaries have associated with them a space charge region whose width is given by[31]

$$W = \left\{ \frac{8\sin(\theta/2)}{\pi bn} \left[\frac{1}{1 - \exp((E_d - E_f)/kT)} \right] \right\}^{\frac{1}{2}} \qquad (5.11)$$

where θ is the angle between the grains, b is the magnitude of the burgers vector, n is the net carrier concentration, and E_d and E_f are the dislocation energy level and the Fermi level respectively. For small grains with large angle grain boundaries this width can exceed the grain size in which case the potential barrier mechanism would no longer be valid.

The space charge width at room temperature for InSb with a net carrier concentration of 3×10^{17} cm^3 and a boundary angle of 10° is ~ 400 $\overset{o}{A}$. This indicates that small grain films can be completely depleted of carriers due to the space charge around the grain boundary. This effect would tend to reduce the mobility very rapidly as the film grain size is decreased to the space charge width.

The rapid increase in mobility with increasing substrate temperature shown in Figure 15 can now be explained in terms of the potential barrier model. At low growth temperatures the grain size is on the order of the width of the space charge region associated with the grain boundaries and the mobility is very low. Increasing the film growth temperature increases the grain size until the grain size exceeds the boundary space charge width at which point the mobility rapidly increases with increasing grain size. When the grain size exceeds the boundary space charge width, a linear increase in mobility with increasing grain size is predicted by the potential barrier model, assuming ϕ remains constant.

The mobility data as a function of growth temperature given in Figure 15 for films grown with deposition rates of 450 $\overset{o}{A}$/min was controlled by the same scattering mechanism. However, in this case the grain size and boundary angles are such that the barrier width is greater than the barrier separation for all growth temperatures investigated and hence the mobility remains low.

The dominant charge scattering mechanism in the films was identified as potential barrier scattering at grain boundaries. The potential barrier energy was determined to be 0.04 eV in excellent agreement with measurements on the potential barrier energy in InSb films deposited by cathodic sputtering and vacuum evaporation. The grain size was found to be limited by the film thickness. Electron mobilities of several hundred cm^2/ V-sec were obtained with 1800 Å thick films on p-a CaF_2 substrates.

REFERENCES

1. J. L. Richards, P. B. Hart, and E. K. Mueller, Single-Crystal Films, edited by M. H. Francombe and H. Sato, Pergamon Press, New York, 1964, pp. 241-249.

2. K. G. Guenther, Z. Naturforsch, 13a, 1081 (1958).

3. H. H. Wieder, Solid-State Comm. 3, 159 (1965).

4. C. Moulton, Nature 195, 793 (1962).

5. H. H. Wieder, Intermetallic Semiconducting Films, Pergamon Press, New York, 1970, pp. 2-73.

6. J. Cervenak, A. Zivcakova, and J. Buch, Czech. J. Phys. B20, 84 (1970).

7. J. Cervenak, Czech. J. Phys. B18, 1449 (1968).

8. I. H. Khan, Surface Sci. 9, 306 (1968).

9. W. Eckenbach, W. Fuhs, and J. Stuke, J. Non-Crystalline Solids 5, 264 (1971).

10. C. H. Ling, J. H. Fisher, and J. C. Anderson, Thin Solid Films 14, 267 (1972).

11. A. R. Clawson, Thin Solid Films 12, 291 (1972).

12. E. Krikorian and R. Sneed, J. Appl. Phys. 37, 3365, (1966).

13. I. H. Khan, J. Appl. Phys. 44, 14 (1973).

14. G. V. Burton and S. C. M. Day, Thin Solid Films, 10, 11 (1972).

15. R. L. Schalla, N. W. Tideswell and F. D. Coffin, Single-Crystal Films, edited by M. H. Francombe and H. Sato, Pergamon Press, New York, 1964, pp. 301-313.

16. W. J. Williamson, Solid-State Electronics 9, 213 (1966).

17. L. J. van der Pauw, Philips Res. Reports 13, 1 (1958).

18. J. J. Cuomo, R. J. Gambino, and R. Rosenberg, J. Vac. Sci. Technol. 11, 34 (1974).

19. F. C. Lou and M. Epstein, Appl. Phys. Lett. 22, 101 (1972).

20. S. S. Lau, R. H. Mills, and D. G. Muth, J. Vac. Sci. Technol. 9, 1196 (1972).

21. C. A. Neugebauer, Handbook of Thin Film Technology, edited by
    L. I. Maissel and R. Glang, McGraw-Hill, New York, 1970, pp. 8-40.

22. K. A. Wickersheim and B. M. Hanking, Physica 25, 569 (1959).

23. R. B. Dzhanelidze and N. I. Kurdiani, Soviet Phys. Solid State
    5, 501 (1963).

24. Chih-Ch'ao Lien and D. N. Nasledov, Soviet Phys. Solid State 3,
    1058 (1960).

25. Y. S. Chiang and G. L. Pearson, J. Appl. Phys. 46, 2986 (1975).

26. H. Flietner, Physica Status Solidi 1, 483 (1961).

27. D. L. Dexter and F. Seitz, Phys. Rev. 86, 964 (1952).

28. H. H. Wieder, Solid State Electronics 9, 373 (1966).

29. R. F. Potter, Phys. Rev. 103, 47 (1956).

30. D. B. Holt, J. Phys. Chem. Solids 27, 1058 (1966).

31. H. F. Matare', Defect Electronics in Semiconductors, Wiley-
    Interscience, New York, 1971, p. 282.

APPENDIX

Glass Substrate Cleaning Procedure

Glass microscope slides, 7059 Corning glass, and fused silica substrates used in the experiments reported in this thesis were cleaned using the following procedure.

1. Ultrasonically agitate the substrates in a detergent solution (Alcanox) for 5 minutes.

2. Rinse in sequential baths of distilled water, methanol, acetone, and trichloroethylene.

3. Ultrasonically agitate in tricholoroethane for 5 minutes.

4. Rinse the substrates in baths of acetone, methanol, and isopropanol.

5. Place the substrates in a boiling isopropanol vapor degreaser.

6. Allow the substrates to cool and then bake them for 10 minutes at 105°C.

Using this procedure, all glass substrates have been found to pass the water break test (ASTM F22-62T). After cleaning, the substrates are immediately placed in the vacuum system.